NATIONAL ADVISORY COMMITTEE FOR AERONAUTICS

SPECIAL REPORT No. 109.

HIGH-SPEED TESTS OF RADIAL-ENGINE COWLINGS

By Russell G. Robinson and John V. Becker
Langley Memorial Aeronautical Laboratory

April 1939

HIGH-SPEED TESTS OF RADIAL-ENGINE COWLINGS

By Russell G. Robinson and John V. Becker

SUMMARY

The drag characteristics of eight radial-engine cowlings have been determined over a wide speed range in the N.A.C.A. 8-foot high-speed wind tunnel. The pressure distribution over all cowlings was measured, to and above the speed of the compressibility burble, as an aid in interpreting the force tests. One-fifth-scale models of radial-engine cowlings on a wing-nacelle combination were used in the tests.

The speed at which the cowling drag abruptly increased owing to the compressibility burble was found to vary from 310 miles per hour for one of the existing shapes to 480 miles per hour for the best shape developed as a result of the present investigation. The corresponding speeds at 30,000 feet altitude in a standard atmosphere (-48° F.) are 280 and 430 miles per hour, respectively. Correlation between the peak negative pressure on the surface of a cowling and the critical speed of the cowling was established. The speed at which the cowling drag abruptly increased was found to be equal to, or slightly greater than, the flight speed at which the speed of sound is reached locally on the cowling. An approximate relationship between the critical speed and the radius of curvature of the nose portion of a cowling is presented. The criterion for the design of low-drag cowlings with high critical speeds appears to be small negative pressures of uniform distribution over the cowling nose, indicative of local velocities that exceed the general stream velocity by a minimum amount. The cowlings developed on this principle had not only the highest critical speeds but also the lowest drags throughout the entire speed range and greater useful ranges of angle of attack.

INTRODUCTION

Experimental work on bodies of many shapes at high speeds has shown that for each shape a speed is reached at which a compressibility burble occurs, causing an abrupt increase in drag and causing, on lifting bodies, a loss of lift and a marked increase in pitching moment. The nature of the compressibility burble is described in reference 1, where it is shown that a compression shock forms on a body

when the local air speed over any part of the body exceeds the local speed of sound. The flight speed at which the local speed of sound is reached is therefore the limiting speed below which the aerodynamic characteristics of a body may be expected to vary in a regular manner and is termed "critical" speed. This critical speed, dependent on the shape and the lift of the body, usually lies between 0.4 and 0.9 the speed of sound, or 305 to 686 miles per hour in standard sea-level atmosphere. The compression shock occurring after the critical speed is reached involves a sudden, rather than a gradual, retardation of the air that has reached supersonic speeds near the surface of the body and results in a dissipation of energy. The source of the increased drag observed at the compressibility burble is the compression shock and the excess drag is due to the conversion of a considerable amount of the air-stream kinetic energy into heat at the compression shock. The drag increases still further at speeds above the compressibility burble because both the intensity (pressure drop) and the extent of the shock measured perpendicular to the body surface increase with increasing speed.

The effect of the drag increase, due to the compression shock, on airplane performance is practically to limit the maximum speed of an airplane to the lowest critical speed of any of its large component parts because of the excessive power required to overcome the drag at higher speeds. The desirability of determining the critical speeds of component parts of an airplane, especially those contributing the most drag and those with the lowest critical speed, is apparent.

Reference 2 supports the reasoning that blunt bodies or bodies of high curvature (e.g., circular cylinder as compared with airfoil sections) have the lowest critical speeds because the maximum local air speed near the surface of such bodies reaches the local speed of sound at a comparatively low free-stream speed. Radial-engine cowlings fall in this class and, fortunately, there are complete pressure-distribution results available to indicate the magnitude of the maximum speed over a number of typical practical cowlings. The results of experimental work on full-scale cowlings tested on an operating engine are given in reference 3. The pressure-distribution data from that reference indicate that two of the cowlings had local speeds over the nose portion approximately twice the magnitude of the free-stream speed. The critical speed of such cowlings, as predicted by the known peak negative

pressure and the relation, presented in reference 4, between the peak pressure and the critical speed, is about 300 miles per hour. Reference 3 also shows the direct effect of curvature of the cowling nose on the peak negative pressure, and hence on maximum local speed over the cowling. This effect suggests increasing the critical speed of a radial-engine cowling by a proper distribution of the curvature.

Reference 3 further shows that the effect of a propeller operating at high-speed or cruising condition does not appreciably alter the peak negative pressure over a cowling in the slipstream. This result is to be expected because at high speeds the propeller slip is very small compared with the forward speed. The critical speed of a cowling under service operating conditions may therefore be determined quite accurately by the use of a model without a propeller.

The purpose of the present investigation was to determine in the high-speed range the merit of models of five full-scale cowlings and new cowling shapes developed from the test results of the first five. Results of the tests were to be correlated to allow the prediction of the compressibility burble from low-speed pressure measurements or from the shape of the cowling.

APPARATUS AND METHOD

The N.A.C.A. 8-foot high-speed wind tunnel in which the investigation was carried out is a single-return, circular, closed-throat tunnel. The flow in the test section has been found by surveys to be satisfactorily steady and uniform both in speed and direction. The air speed is continuously controllable from 75 to more than 500 miles per hour. The turbulence, as determined by sphere tests (reference 5), is approximately equivalent to that of free air. T. F. = 1.00 –

The radial-engine cowlings were mounted on a nacelle which, in turn, was mounted centrally on a wing of 2-foot chord and N.A.C.A. 23012 section. The wing completely spanned the test section of the tunnel. The cowlings and the nacelle were one-fifth the size of the full-scale cowlings and nacelle reported in reference 3. The wing was metal-covered, unpainted, and aerodynamically smooth; that

is, further polishing would produce no decrease in profile drag. Figure 1 is a cross-sectional view through the center of the wing-nacelle combination. A general view of the nacelle with cowling nose 1 and skirt 1 is shown in figure 2. Figure 3 shows the wing-nacelle assembly mounted in the tunnel.

One-fifth-scale (10.40-inch diameter) cowling models were chosen as the largest that could be used with the 2-foot-chord wing and still maintain normal wing-nacelle proportions. The ratio

$$\frac{\text{cowling diameter}}{\text{wing chord}} = 0.43$$

for the model, is somewhat larger than for average practice but is within the range of present-day installations. The center line of the nacelle lay on the chord line of the wing. The fore-and-aft position of the nacelle was such as to locate the propeller, had there been one, 40 percent of the wing chord ahead of the leading edge.

The five cowling-nose shapes (fig. 4) scaled down from the corresponding full-scale cowlings employed in the investigation reported in reference 3 are designated by the same numbers used in that investigation. Nose 1 was modified progressively by cutting back to larger radii at the leading edge. Noses A, B, and C were designed as the tests progressed. They have the same over-all dimensions as nose 2 but have different intermediate ordinates. Figure 5 presents photographs of nose 5 and and nose C. A blank nose with a square corner and the same over-all dimensions as nose 2 was also tested. Table 1 gives the ordinates for all the cowling noses tested.

TABLE I

Values of R in Inches for 8 Model Noses of 10.40-Inch Diameter Cowling

(See figs. 1 and 4.)

x (in.)	Nose								
	1	2	4	5	7		A	B	C
					Outside	Inside			
0.00	4.40	3.64	4.48	4.36	4.29	4.29	3.64	3.64	3.64
.05	4.50	3.79	4.75	4.61	4.47	4.13	3.76	3.87	3.93
.10	4.53	3.88	4.84	4.70	4.56	4.06	3.84	3.97	4.02
.20	4.59	4.05	4.96	4.88	4.68	4.00	3.96	4.11	4.15
.40	4.70	4.32	5.09	5.05	4.87	3.98	4.16	4.31	4.33
.60	4.79	4.52	5.15	5.13	4.98	-	4.34	4.47	4.48
.80	4.85	4.67	5.18	5.17	5.07	-	4.48	4.59	4.59
1.00	4.91	4.79	5.19	5.18	5.13	-	4.60	4.70	4.70
1.20	4.96	4.88	5.20	5.19	5.16	-	4.71	4.80	4.78
1.40	5.00	4.96	5.20	5.20	5.18	-	4.81	4.87	4.86
1.60	5.04	5.03	5.20	5.20	5.19	-	4.90	4.94	4.93
2.00	5.10	5.11	5.20	5.20	5.20	-	5.03	5.04	5.05
2.40	5.14	5.14	5.20	5.20	5.20	-	5.12	5.12	5.13
2.80	5.18	5.18	5.20	5.20	-	-	5.18	5.17	5.18
3.20	5.20	5.20	5.20	5.20	-	-	5.20	5.19	5.20
3.23	5.20	5.20	5.20	5.20	-	-	5.20	5.20	5.20
3.48	5.20	5.20	5.20	5.20	-	-	5.20	5.20	5.20

Two cowling skirts were employed in the investigation. Ordinates of the nacelle, which is similar to nacelle 2 of reference 3, are given in table II.

TABLE II

Nacelle-Model Ordinates

(See figs. 1 and 4.)

L (in.)	R (in.)
0.00	1.94
.25	2.02
.65	2.30
1.05	2.69
1.25	2.92
1.45	3.18
1.65	3.47
1.85	3.75
2.05	3.98
2.25	4.17
2.65	4.48
3.05	4.73
3.45	4.92
3.85	5.04
4.25	5.12
4.75	5.16
5.25	5.17
6.25	5.11
7.25	5.01
8.25	4.86
10.25	4.47
12.25	3.98
14.25	3.30
16.25	2.56
18.25	1.75
19.25	1.31
20.25	.87

All the cowlings were tested with a controlled amount of cooling air through them. A flat baffle plate with 16 15/16-inch holes simulated a baffled radial engine of conductivity K (reference 3), or equivalent leak area, approximately 9 percent. The baffle plate was incidentally used to support the replaceable nose and skirt portions, which were of cast nickel-iron and were finished smooth and flush.

A pressure drop of 30 pounds per square foot across

the engine or baffle plate was used as a criterion of satisfactory cooling conditions, cowling skirt 1 provided an exit-slot opening of 0.25 inch and the required pressure drop for cooling at speeds of the order of 200 miles per hour. Cowling skirt 2 provided an exit opening of 0.11 inch (0.55 inch on full-scale engine cowling) and proper cooling at speeds of the order of 300 miles per hour.

The pressure distribution over the top of each cowling was measured at seven static-pressure orifices (fig. 1). The orifices were located according to the expected pressure distribution for the particular cowling, several tubes being located near the point of peak negative pressure. The locations are given in table III.

A total-pressure tube was located above the cowling skirt near its trailing edge (see figs. 1 and 5) for detecting any loss, such as that of a compression shock, outside the boundary layer. A total-pressure tube and a static-pressure tube were placed in the center of the exit opening on the top side of the nacelle for measuring the air speed and the total pressure in the exit opening.

All the cowlings were tested over a speed range extending from 115 miles per hour to a speed greater than the critical speed for each model at angles of attack of -1° and 0°. Owing to structural limitations of the wing, the maximum air speed was limited to 425 miles per hour at 1° and to 275 miles per hour at 2°. Noses 1-f, 5, and B, which were considered representative of the several types investigated, were tested through a range of angles of attack of -3° to 6° at 230 miles per hour. All the models were tested with skirt 1; only nose 5 was tested with skirt 2.

The lift, the drag, and the pitching moment of the wing-nacelle-cowling combinations were measured at intervals of 30 miles per hour at the lower speeds and more frequently near the critical speeds. The characteristics of the wing alone were determined in the same way. Pressure measurements on the cowlings were made simultaneously with the force measurements.

TABLE III

Location of Pressure Orifices on Cowlings

(See fig. 1.)

Nose	Orifice													
	1		2		3		4		5		6		7	
	x (in.)	R (in.)	x (in.)	R (in.)	x (in.)	R (in.)	x (in.)	R (in.)	x (in.)	R (in.)	x (in.)	R (in.)	x (in.)	R (in.)
1	0.01	4.41	0.04	4.49	0.23	4.62	0.80	4.85	1.60	5.04	2.75	5.17	5.18	5.20
2	.25	4.09	.70	4.60	1.16	4.86	1.70	5.05	2.25	5.13	3.00	5.19	5.18	5.20
4	0	4.50	.10	4.84	.25	4.99	.45	5.11	.69	5.17	2.00	5.20	5.18	5.20
5	.03	4.49	.20	4.88	.35	5.00	.50	5.11	.90	5.19	2.00	5.20	5.18	5.20
7	0	4.29	.10	4.56	.35	4.80	.65	5.01	1.00	5.13	1.50	5.19	5.18	5.20
A	.25	4.01	.70	4.40	1.16	4.67	1.70	4.91	2.25	5.08	3.00	5.19	5.18	5.20
B	.25	4.17	.70	4.53	1.16	4.78	1.70	4.97	2.25	5.09	3.00	5.18	5.18	5.20
C	.25	4.20	.70	4.54	1.16	4.76	1.70	4.96	2.25	5.10	3.00	5.19	5.18	5.20

RESULTS

Compressibility effects, such as those encountered at high speeds on the engine cowlings under consideration, are intimately connected with the nondimensional Mach number M in the same way that scale effects are connected with the Reynolds Number R. Mach number M is the ratio of air speed V to the speed of sound in the air c. Results in this report are plotted against M.

Given the temperature of the air, the air speed corresponding to a given Mach number M may be found from

$$V = Mc$$

and

$$c = 33.5\sqrt{460 + t}$$

where t is the temperature in Fahrenheit degrees and V and c are in miles per hour.

In some cases, for ease in visualizing the magnitude of the speeds, a scale of air speed for standard sea-level conditions ($t = 59^\circ$ F., $c = 763$ miles per hour) is included in the figures.

The drag coefficients and the pressure coefficients are computed using the dynamic pressure $q(= \frac{1}{2}\rho V^2)$ in accordance with standard aeronautical practice. The results, as presented, then indicate directly all compressibility effects.

Force Tests and Pressure-Distribution Measurements

The results are presented in terms of nondimensional coefficients. Figure 6 shows the relative magnitude of the drag force of the wing alone and the wing-nacelle combination (both uncorrected for tunnel-wall effects). The drag coefficients for this figure are based on wing area:

$$C_D = \frac{\text{drag of wing + nacelle}}{q \times 15.35}$$

For use in the comparison of the drags of various cowlings, an effective nacelle drag coefficient C_{D_F} based on the frontal area of the cowling (0.590 square foot) is used.

This coefficient, of course, includes the drag and the interference of the nacelle. By definition:

$$C_{D_F} = \frac{\text{effective nacelle drag}}{q \times 0.590}$$

$$= \frac{(\text{drag of wing + nacelle}) - (\text{drag of wing alone})}{q \times 0.590}$$

Effective nacelle drag coefficients for the cowling noses 2, 4, 5, 7, A, B, and C with skirt 1 are shown in figure 7. The results obtained with nose 1 and with several modifications of nose 1, together with those for the square-corner blank nose, are shown in figure 8. Figure 9 shows the results of the test of nose 5 with skirt 2. The curves of effective nacelle drag coefficient were obtained from faired curves of the drag of the wing alone and the drag of the wing-nacelle combination for the same angle of attack.

The pressure distribution over the nose section of a cowling is plotted in terms of the pressure coefficient P

$$P = \frac{p - p_\infty}{q}$$

where p is the local ststic pressure.

p_∞, static pressure in the free stream.

q, dynamic pressure, $\frac{1}{2} \rho V^2$.

The value of P is then a measure of the local speed over the nose. In accordance with Bernoulli's equation $P = 0$ indicates a speed equal to the free-stream speed, positive values indicate less than free-stream speed, and negative values indicate more than free-stream speed. The pressure-distribution diagrams for the models at various angles of attack, at $M = 0.30$, are shown in figure 10(a) to (i). Figure 10(j) shows an effect of the compressibility burble on the pressure distribution. Typical variation with M of the static pressure at each of the seven orifices is shown in figure 11 for noses 4, 7, and B at angles of attack of 0° and 1°. The loss in total pressure ΔH between the free stream and the total-pressure tube at the rear of the cowling is shown in figure 12 for noses 4, 5, 7, A, and B for angles of attack of 0° and 1°.

Cross plots of effective nacelle drag coefficient C_{D_F} against angle of attack α for $M = 0.30$ are shown in figure 13 for cowling noses 1-f, 5, A, B, and C. The corresponding variation in pressure coefficient P is shown in figure 14 for noses 5 and B.

Figure 15 presents a comparison of the lift curve for the wing-nacelle combination with that of the wing alone. Lift coefficients are based on the wing area of 15.35 square feet:

$$C_L = \frac{\text{lift of wing + nacelle}}{q \times 15.35}$$

There was no measurable difference in lift for the different noses. Figure 16 shows the effect on wing pitching moment of the presence of the nacelle. The pitching-moment coefficient is based on the wing chord of 2 feet:

$$C_{m_{c/4}} = \frac{(\text{moment of wing + nacelle})_{c/4}}{q \times 15.35 \times 2}$$

The results presented in figures 15 and 16 are uncorrected for tunnel-wall effects and therefore should be used only qualitatively.

Cooling

The pressure drop available for cooling across an engine or baffle plate has been shown (reference 3) to be nearly equal to the loss in total pressure between the free stream and the exit opening of the cowling skirt. This loss and the exit speed were measured at only one point in the exit opening of the cowlings under test and, because of the flow variation around the exit opening induced by the presence of the wing, these measurements give only approximations of the conditions existing over the entire cowling. The measured values, however, indicate that the design conductivity K of 9 percent was attained and that the specified pressure drop of 30 pounds per square foot was attained at about 200 and 300 miles per hour with skirt 1 and skirt 2, respectively. There was no measurable variation with speed of the ratio

$$\frac{\text{pressure drop across baffle plate}}{\text{dynamic pressure}}$$

PRECISION

The force-test data presented in this report are uncorrected for tunnel-wall effects. The tunnel-wall effect on a wing extending across the throat of a closed tunnel is appreciable but has not yet been determined for this wind tunnel. This factor is believed, however, to have a negligible influence on the effective nacelle drag owing to the small lift changes involved (see fig. 15) and the small induced drag of a wing spanning a closed tunnel. The effect of the tunnel wall on the critical speed of a body has not been determined but it is believed to be of secondary importance when, as in the present case, the cross section of the body is of the order of 1 percent of the cross-sectional area of the jet. The horizontal buoyancy correction for static-pressure gradient is of the order of one-half percent of the effective nacelle drag and is therefore neglected.

The average scatter of the test data for the wing alone and the wing-nacelle combinations indicates random errors in force measurement, based on the wing area, as follows:

C_L, ± 0.003

$C_{m_{c/4}}$, ± 0.0005

C_D, ± 0.0001

M, ± 0.01

This error in drag coefficient represents about 4 percent of the effective nacelle drag of nose C, which had the least drag of the models tested. Inasmuch as the same wing drag was subtracted from the drag of each combination, the precision for comparing cowlings is equal to the error just discussed; absolute values for any cowling will be subject, in addition, to the errors in determining the characteristics of the wing alone and therefore will be subject to errors twice as great.

DISCUSSION

Correlation of Drag and Pressure-Distribution Measurements

Figure 7 indicates the speed at which the drag of each cowling increases excessively because of the presence of a compression shock and also the magnitude of the drag change under such conditions. The results indicate that it would be impractical to employ any cowling at flight speeds greater than the speed at which a compression shock forms on the cowling. The bluntest cowlings (4 and 5) are satisfactory for speeds of the order of 300 miles per hour; one of the standard shapes (nose 2) and all of the new shapes developed in this investigation are satisfactory up to about 480 miles per hour (all speeds at sea level, 59° F.).

The critical speed at which the local speed of sound was actually reached on each cowling nose has been computed for all the cases in which the peak negative pressure was measured; the speed is shown by a tick on the curves of figures 7(a) and 7(c). It is seen that, for noses 2, 4, and 7, the compressibility burble did not occur until the critical speed had been exceeded by about $M = 0.03$; that is, the speed of sound was exceeded locally before a measurable shock occurred on these noses. For noses 5, A, B, and C, the shock apparently formed almost immediately after the critical speed was reached. Since noses 2, 4, and 7 have no common geometric characteristic, the present tests indicate no controlling factor that permits the local speed to exceed the local sonic speed before a compression shock occurs and it must therefore be concluded that any cowling is likely to experience a compressibility burble as soon as the local speed reaches the speed of sound. The critical speed determined on this basis should be used as the upper limit of the flying speed for a radial-engine cowling. The upper limit of the useful speed range for the cowlings tested is then from $M = 0.413$ to $M = 0.625$, or 310 to 480 miles per hour at sea level (59° F.).

As previously discussed, the critical speed in miles per hour V_{crit} is dependent on the atmospheric temperature. That is,

$$V_{crit} = M_{crit}\, c$$

where

$$c = 33.5 \sqrt{460 + t} \text{ miles per hour}$$

The temperature of the standard atmosphere decreases with altitude to -67° F. at about 35,000 feet. The decrease in temperature causes a decrease in the speed of sound c with increasing altitude and results in lower critical speeds as altitude increases. At 30,000 feet the critical speeds for the cowlings tested are lowered to the range of 280 to 430 miles per hour. Since the flying speed of present-day airplanes generally increases with altitude, the danger of encountering serious compressibility effects is very real unless proper care is taken in designing the cowling nose.

As was to be expected, the cowlings with the greatest negative pressure (e.g., noses 4 and 5, figs. 10(c) and (d)) had the lowest critical speeds. Also, as would be expected, the pressure measurements (fig. 10) showed larger peak negative pressures for angles of attack other than zero, the increment due to angle of attack being approximately proportional to the angle change and being greater for cowlings on which the pressure already had a large negative value. The critical speed should be lower, then, when a cowling is pitched or yawed, especially for noses like 4 and 5; the results presented in figures 7(b) and 7(c) confirm this conclusion. This behavior illustrates the importance of alining the cowling with the air direction when the airplane is in the high-speed attitude, especially if the cowling is blunt or is near its critical speed.

The rapid increase in drag of noses 4 and 5 at air speeds below 200 miles per hour for 2° angle of attack (fig. 7(d)) is not to be attributed to the compressibility burble. The pressure diagrams (figs. 10(c) and 10(d)) show radical changes in pressure distribution and show small peak negative pressures at 2° angle of attack, indicating a flow breakdown; but, from the fact that the maximum local speeds were less than half sonic speed before the change in flow occurred, the breakdown is attributed to ordinary stalling over the top of the cowling and not to a compressibility burble. This effect is discussed in detail later.

The curves of figure 11 show the way in which the static pressure over typical cowlings varies as the speed is increased above the critical speed, but they fail to show uniform tendencies for all cowlings above the critical

M. The blunter cowlings show a decided reduction in the magnitude of the negative pressure coefficients but the reduction occurs at a value of M appreciably higher than the critical value. The cowlings of better shape show a less decided change in pressure coefficient above the critical speed and, in some cases, even an increase in negative pressure (fig. 11(d)). These results indicate that static-pressure measurements are not always a reliable or an accurate means of detecting the presence of a compression shock. Figure 10(j) shows to what extent the pressure distribution may be altered by the compressibility burble. All these results point to the practical conclusion that, if the structural design of a cowling is based on low-speed pressure-distribution data with values suitably increased for compressibility (see fig. 11) to flight speed or critical speed, only a small additional allowance is necessary for the negative pressure developed after the critical speed is exceeded.

The total-pressure measurements of figure 12 also show marked effects for the blunter cowlings and smaller or negligible effects for the cowlings of better shape. For the blunt cowlings, the loss in total pressure is large and occurs almost immediately after the critical speed is reached; for the better cowlings, the loss occurs later (fig. 12(c)) or is of a negligible magnitude (fig. 12(d)). Although in these tests, the total-pressure tube did not show a loss corresponding to the drag increase of the better cowlings, this result may be attributable to the nature of the shocks on those cowlings. If the shocks extended a considerable distance fore and aft, as would be expected from the nearly uniform pressure distributions, then their extent normal to the surface may have been small and the wake may have passed under the tube. The indication is that a detecting tube must be immediately outside the normal boundary layer.

A theoretical relation between peak negative pressure, as measured at low speed, and critical speed has been obtained by Jacobs (reference 4) by defining the critical speed as usual (maximum local speed equal to local speed of sound) and assuming that the negative pressure coefficients increase with speed according to the ratio $1/\sqrt{1 - M^2}$. This relation is shown by the curve of figure 17. The measured critical speed for each of the cowlings is plotted in figure 17 against the value of its maximum negative pressure coefficient P_{max} extrapolated to zero speed to give

$P_{o_{max}}$. It is evident that, if the low-speed pressure distribution for a cowling design is known from wind-tunnel or flight tests, the curve of figure 17 may be used to obtain a good approximation of the critical speed of the cowling. The low-speed value of P_{max} must, of course, be for the airplane attitude corresponding to the high speed being investigated.

An Approximate Relation between Cowling-Nose Radius of Curvature and Critical Speed

Since the curvature of a cowling controls the peak negative pressure and since the peak negative pressure controls the critical speed, the critical speed may be related to the cowling shape by plotting measured critical speeds against the radius of curvature of the cowling at the position of the peak-pressure point. The radius is made nondimensional by dividing by the radius of the cowling R and the results are plotted as squares in figure 18. In order to make the relation independent of a knowledge of the position of peak negative pressure as well as of a knowledge of the value of the pressure, it is desirable to designate completely the location of the critical radius by the geometry of the cowling. If r is taken as the minimum radius between the 25-percent and the 75-percent points of the curved portion of the cowling nose and the critical speed is taken from the theoretical curve of figure 17, the values shown by the circles of figure 18 are obtained. The general agreement indicates that the critical speed of a cowling similar to those tested may be predicted by the curve of figure 18, having only a line drawing of the cowling profile.

It should be remembered that figure 18 gives directly only the critical speed for zero angle of attack of the cowling axis. For small angles of attack (if stalling is not produced) the amount by which the critical speed will be lowered may be estimated from the pressure changes shown in figure 10 or 14 for the most similar cowling. The speed change corresponding to this pressure change may then be obtained from figure 17. For example, on nose 4 (fig. 10(c)) the peak negative pressure coefficient becomes greater by 0.4 at 1°. In the neighborhood of M = 0.45, the curve of figure 17 indicates the critical speed to be lowered by M = 0.023, or 17 miles per hour at sea level,

for a peak negative pressure increase of 0.4. The drag results show a lowering of the speed at which the shock occurred by $M = 0.025$. Using pressure data from figure 14, similar considerations indicate that, even for nose B, the critical speed will be reduced by $M = 0.13$ for an increase in angle of attack from 0° to 6°. This decrease, about 100 miles per hour at sea level, indicates the importance of knowing the flight attitude and keeping it at the optimum in very high-speed flight.

Effect of Variation of Angle of Attack on Flow over Cowlings

The negative pressures over the nose of a cowling and the change of pressure with angle of attack are very similar to the pressures and changes experienced by airfoil profiles. Reference 3 points out that the flow direction immediately in front of a cowling is more nearly radial than axial. Depending on the relative direction of the oncoming air and the slope of the cowling just back of the leading-edge radius, a cowling nose may be acting similarly to an airfoil (1) at low or zero lift (e.g., noses A, B, C); (2) at high lift (noses 4 and 5); or (3) beyond maximum lift, i.e., stalled (nose 1) as shown by the pressure diagrams of figure 10. This comparison indicates the reason why some cowlings have a greater useful angle range without stalling than others.

In the present test set-up, as in the case of actual nacelles near the center of a wing or even of the engine cowling of a single-engine airplane, the relative angle between the oncoming air and the nose of the cowling is increased by the induced upflow in front of the wing. The effective angle of attack of a cowling always being greater than the geometric angle, a cowling may stall at a comparatively small angle in spite of the fact that it is a body of revolution with three-dimensional flow. The likelihood is greater when large negative pressures are present at zero angle.

Figures 10(c) and (d) show the large negative pressures for noses 4 and 5 at $\alpha = 0^\circ$ and the increase of negative pressure with angle. The stall is seen to have occurred before 2° was reached and apparently a negative pressure of about $P = -3.2$ was the most that could be maintained before the stall occurred. (See fig. 14.) Fig-

ures 10(f), (g), and (h) show the small negative pressures for noses A, B, and C at $\alpha = 0^\circ$; and figures 10 and 14 indicate that the rate of increase of negative pressure with angle was proportionately smaller than for noses 4 and 5. If a pressure coefficient P of about -3.2 is still the limit, these cowlings will have a wide useful range of angle of attack without stalling. Figure 13 corroborates these conclusions in indicating a rise in drag for nose 5 outside the range $\pm 1^\circ$, as expected from the stall; whereas the drag of nose B does not rise correspondingly, even at 6°, which was the limit of the tests. Noses A and C undoubtedly have characteristics similar to B. These effects are important not only for controlling the drag of an airplane for cowling attitudes other than zero but also for air scoops or any other construction depending on smooth flow over the top of the cowling.

Comparative Drag Results

Figure 7 indicates that there was no large variation of the effective nacelle drag with speed until the critical speed was reached; the favorable scale effects were balanced at the higher speeds by the unfavorable compressibility effects. The results show, however, appreciable differences in effective nacelle drag for the various nose forms. With nose 5, the effective nacelle drag was approximately 30 percent greater than with nose C. In general, the noses of low curvature, low peak negative pressure, and low local speeds were superior to those of high curvature and correspondingly high local speeds. The lower skin-friction drag for the models of low local speeds may account in part for the lower drags of noses A, B, and C. A comparison of the pressure-distribution curves for noses 2, A, B, and C (fig. 10) shows the extent to which the peak negative pressures were lowered and the pressure, or the velocity, distribution made more uniform by successive changes in nose curvature. The reduction in drag from nose A to nose C is probably due to decreasing the pressure (increasing the speed) over the forward portion of the nose, thereby reducing the form drag, or increasing the thrust of the nose.

Figure 19 shows a relation, heretofore unpublished, between the effective nacelle drag and the ratio of wing thickness to cowling diameter as reported for similar nacelles in references 6 and 7. The drags are larger than for the present tests because of the higher conductivity

and the larger skirt opening used in the earlier tests, but the trend of the curve may be used as a guide in extrapolating the present results to other ratios of wing thickness to cowling diameter, as indicated by the dotted lines.

The drag savings that may be effected by passing exactly the correct quantity of cooling air through a cowling at every speed instead of using openings and exits of fixed size for the entire speed range have been previously discussed (reference 3). The results presented by figure 20 show quantitatively the drag differences between cowlings designed to operate with proper engine cooling at 200 and 300 miles per hour, the difference representing the wasted drag caused by the excess cooling air when a cowling with openings sufficient for 200 miles per hour is flown at 300 miles per hour. The fact that the cowling with the smaller exit opening (skirt 2) shows a lower critical speed at $\alpha = 0^\circ$ suggests that a part of the air which formerly passed inside the cowling (with the larger exit opening) now passes outside the cowling to increase the local speed on the cowling nose. The increased speed outside the cowling, or the equally important factor of increasing angle of relative wind at the cowling nose with reduced flow through the cowling, also appears as a detrimental effect in reducing the useful angle-of-attack range of a cowling; with nose 5, the cowling stalled at 1°. (Cf. figs. 10(d) and 10(i).) The lower critical speed and the smaller useful angle-of-attack range both emphasize the relative importance of using the best possible nose shape when the internal flow is most restricted, as is the case in high-speed flight with the optimum amount of cooling air.

The effective nacelle drag for nose 1 (fig. 8) and the pressure distribution (fig. 10(a)) both indicate that this nose was stalled at all angles of attack, including 0°. An attempt was made to improve the flow over the nose by successively cutting back the nose to form profiles with circular arcs of larger radii inscribed in the leading edge on the assumption that a radius would be reached at which the flow would be unstalled. The drag for each modification, however, was found to be larger than for the preceding condition. The change in drag with increase of angle of attack for nose 1-f, as shown in figure 13, indicates that the decrease in effective angle of attack on the bottom of the cowling caused a considerable improvement in the flow at that point which was not at first coun-

teracted by increased severity of the stall on top of the cowling. The modifications to nose 1 were ineffective, probably because the slope of the chord line of the nose decreased as the nose radius was increased; in critical cases, it appears to be much more important to aline the slope of the nose with the relative wind than to increase the nose radius.

CONCLUSIONS

1. The speeds at which the nacelle drag abruptly increased owing to the compressibility burble ranged from 310 to 480 miles per hour at sea level (59° F.) for the cowlings tested. Because of the decrease in the speed of sound with decreasing temperature, the corresponding range at 30,000 feet altitude (-48° F.) would be 280 to 430 miles per hour.

2. The nacelle drag increased so rapidly beyond the critical speed that airplane maximum speeds would be practically limited to the critical speed of the cowling.

3. The pressure distribution over any cowling nose, as measured in flight at ordinary speeds or in a wind tunnel at low speed, may be used to predict the critical speed of the cowling.

4. A close approximation of the critical speed of any cowling similar to those tested may be obtained from the presented relationship between the radius of curvature of the cowling nose and the critical speed.

5. The criterion for a cowling designed to have a high critical speed appears to be uniform, and small, negative pressures over the nose. This condition indicates a speed over the entire nose that is constant and exceeds the general stream speed by a minimum amount.

6. The cowlings developed to have the highest critical speeds also had the lowest drags throughout the entire speed range and had a greater useful angle-of-attack range without an increase in drag.

Langley Memorial Aeronautical Laboratory,
National Advisory Committee for Aeronautics,
Langley Field, Va., March 30, 1939.

REFERENCES

1. Stack, John: The Compressibility Burble. T.N. No. 543, N.A.C.A., 1935.

2. Lindsey, W. F.: Drag of Cylinders of Simple Shapes. T.R. No. 619, N.A.C.A., 1938.

3. Theodorsen, Theodore, Brevoort, M. J., and Stickle, George W.: Full-Scale Tests of N.A.C.A. Cowlings. T.R. No. 592, N.A.C.A., 1937.

4. Jacobs, Eastman N.: Methods Employed in America for the Experimental Investigation of Aerodynamic Phenomena of High Speeds. Misc. Paper No. 42, N.A.C.A., 1936.

5. Robinson, Russell G.: Sphere Tests in the N.A.C.A. 8-Foot High-Speed Tunnel. Jour. Aero. Sci., vol. 4, no. 5, March 1937, pp. 199-201.

6. Wood, Donald H.: Tests of Nacelle-Propeller Combinations in Various Positions with Reference to Wings. Part I. Thick Wing - N.A.C.A. Cowled Nacelle - Tractor Propeller. T.R. No. 415, N.A.C.A., 1932.

7. Wood, Donald H.: Tests of Nacelle-Propeller Combinations in Various Positions with Reference to Wings. III - Clark Y Wing - Various Radial-Engine Cowlings - Tractor Propeller. T.R. No. 462, N.A.C.A., 1933.

FIGURE LEGENDS

Figure 1.- Assembly of wing, nacelle, and cowling. Nose C, skirt 1.

Figure 2.- Wing-nacelle combination. Nose 1, skirt 1.

Figure 3.- Rear view of wing nacelle combination mounted in the tunnel.

Figure 4.- Cowling profiles.

(a) Nose 5 (b) Nose C
Figure 5.- Model cowlings.

Figure 6.- Drag of wing and wing-nacelle combinations. Uncorrected for tunnel-wall effects. α, -1°.

(a) α, 0° (b) α, -1° (c) α, 1° (d) α, 2°
Figure 7.- Effective nacelle drag for various noses, skirt 1. The ticks indicate the critical M.

Figure 8.- Effective nacelle drag for nose 1, modifications to nose 1, and blank nose. α, 0°.

Figure 9.- Effective nacelle drag for nose 5, skirt 2. The tick indicates the critical M.

(a) Nose 1, skirt 1 (b) Nose 2, skirt 1 (c) Nose 4, skirt 1
(d) Nose 5, skirt 1 (e) Nose 7, skirt 1 (f) Nose A, skirt 1
(g) Nose B, skirt 1 (h) Nose C, skirt 1 (i) Nose 5, skirt 2
(j) Nose 5, skirt 2; critical M = 0.46; $\alpha = 0^\circ$
Figure 10.- Pressure distribution over top of cowlings. M = 0.30, except as noted.

(a) Nose 4; α, 0°; critical M, 0.413
(b) Nose 4; α, 1°; critical M, 0.398
(c) Nose 7; α, 0°; critical M, 0.494
(d) Nose B; α, 0°; critical M, 0.624
Figure 11.- Variation with speed of pressures over top of cowlings.

(a) Nose 4, skirt 1 (b) Nose 5, skirt 2
(c) Nose 7, skirt 1 (d) Noses A and B, skirt 1
Figure 12.- Variation with speed of loss of total pressure in rear of cowlings.

Figure 13.- Variation with angle of attack of effective nacelle drag. M, 0.30.

(a) Nose 5, skirt 1. (b) Nose B, skirt 1.

Figure 14.- Variation with angle of attack of pressures over top of cowlings. M, 0.30.

Figure 15.- Effect of nacelle on wing lift. Uncorrected for tunnel-wall effects. M, 0.30.

Figure 16.- Effect of nacelle on wing pitching moment. Uncorrected for tunnel-wall effects. M, 0.30.

Figure 17.- Variation of critical speed with peak-pressure coefficient.

Figure 18.- Relation between radius of curvature of cowling nose and critical speed. α, 0°.

Figure 19.- Variation of effective nacelle-drag coefficient with wing thickness.

Figure 20.- Comparison of effective nacelle drag of nose 5 with skirt 1 and skirt 2.

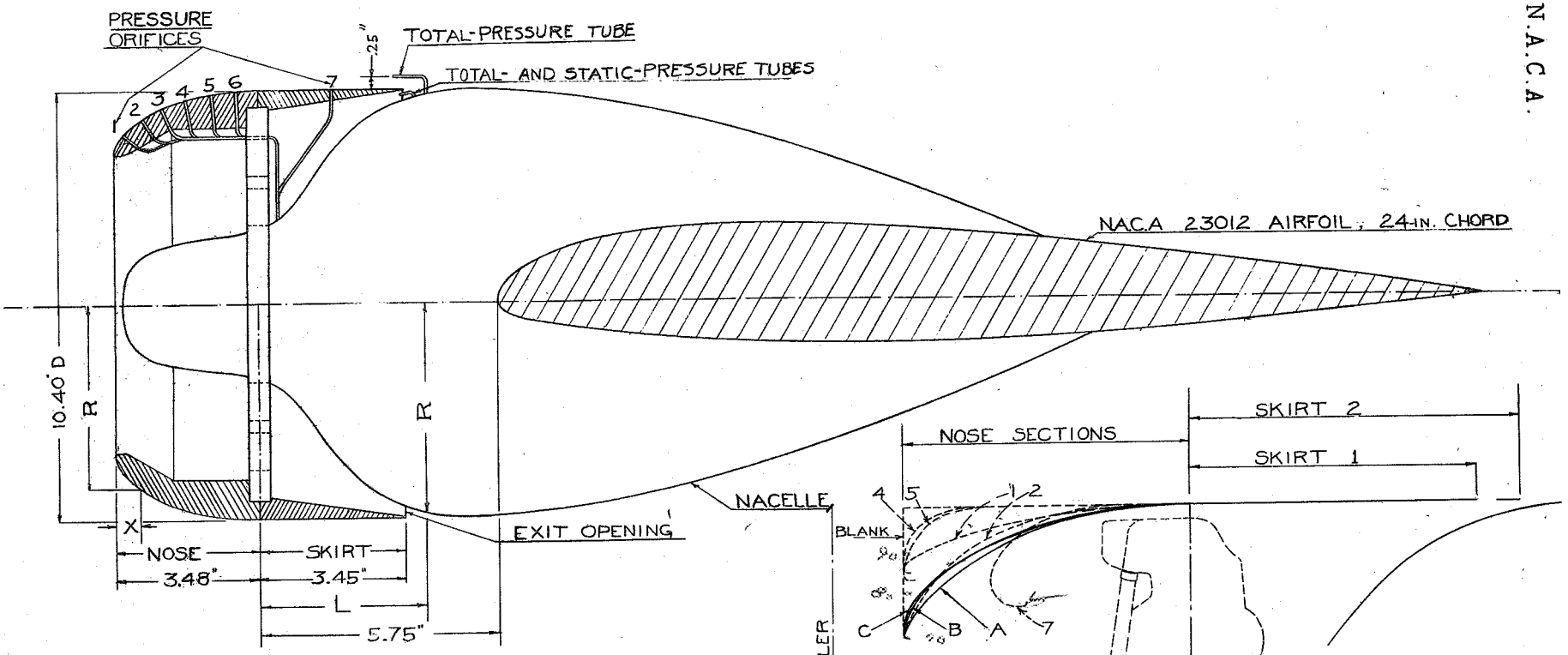

FIGURE 1.- ASSEMBLY OF WING, NACELLE, AND COWLING NOSE C, SKIRT 1.

FIGURE 4.- COWLING PROFILES.

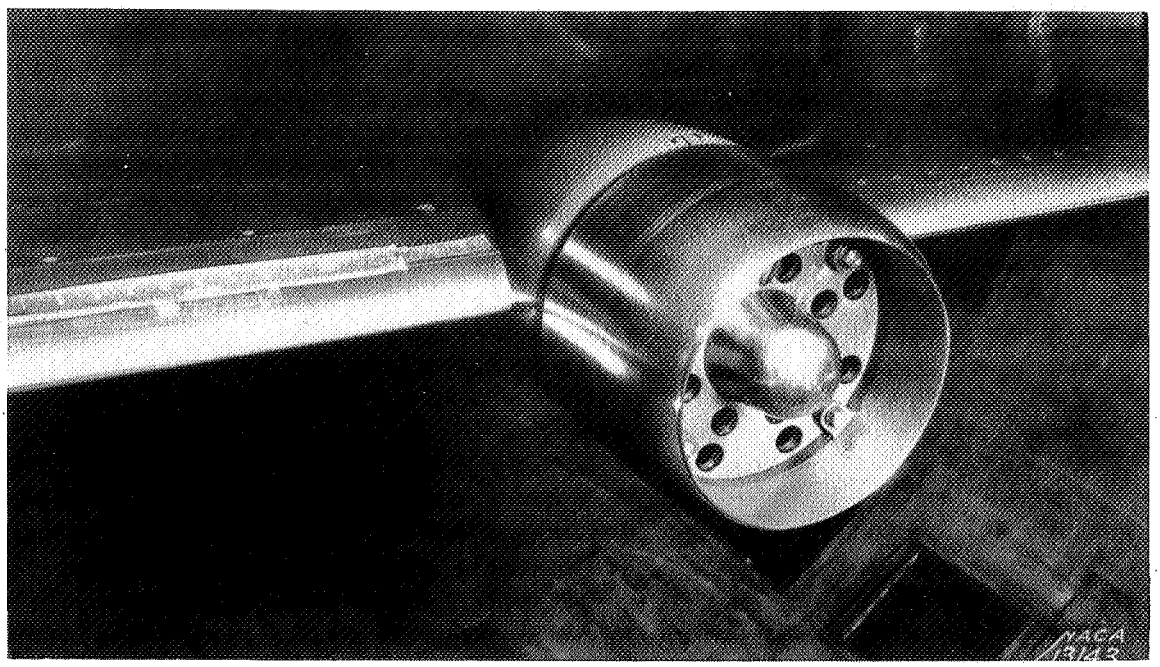

Figure 2

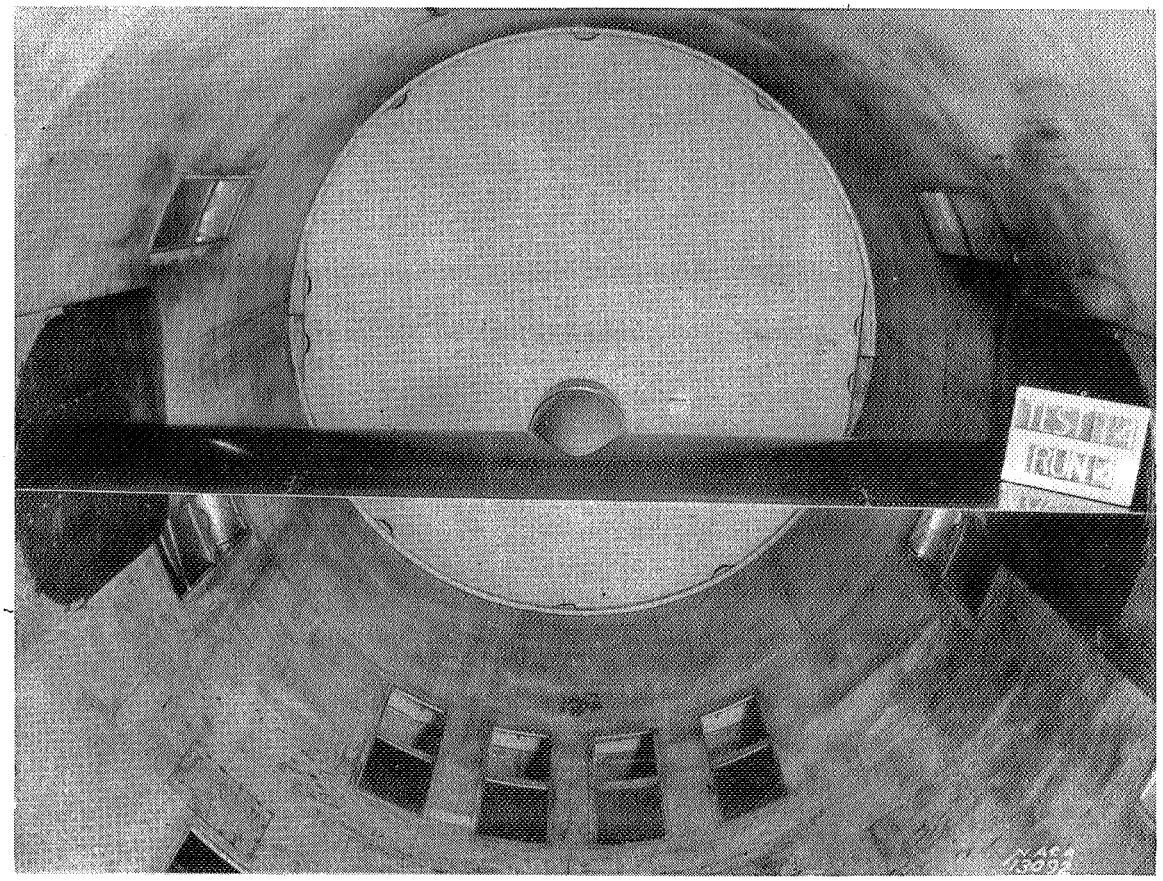

Figure 3

9000
800
14,400,000

Wing RN

Approx. R.N. = $(9354)(764)(2.0)(M)$ (MPH · FT)

$= (14.3)(10^6)(M)$

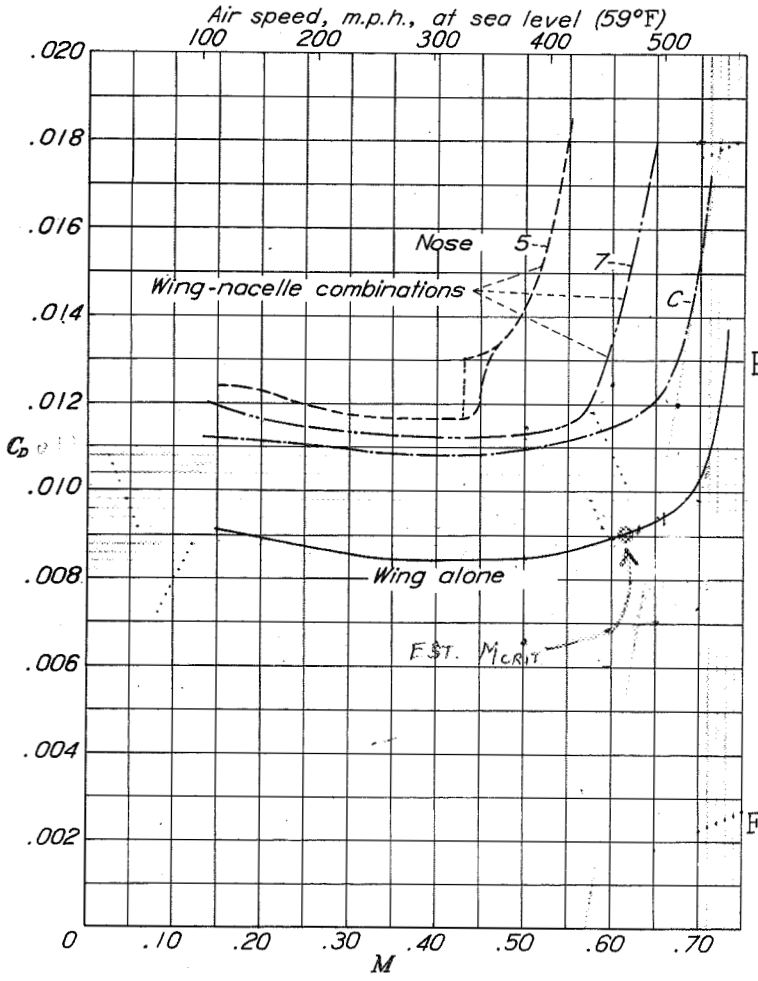

Figure 6

Drag increments for tunnel wall effects. - $\alpha = -1.0°$ $C_L = 0.0$ ($M = 0.30$)

Figure 5a →

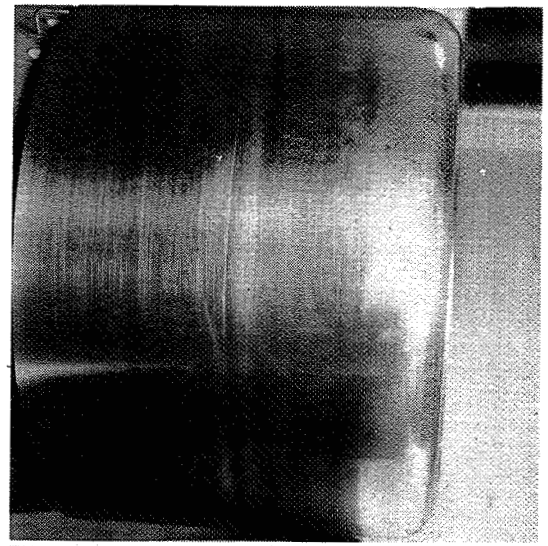

Figure 5b →

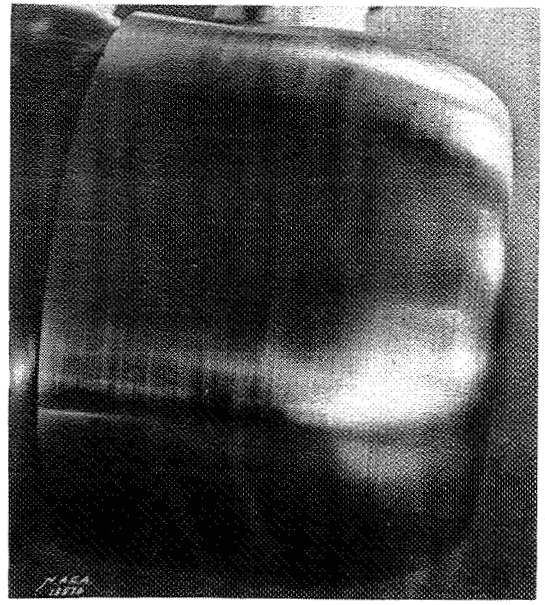

N.A.C.A.

Figs. 5,a,b,6

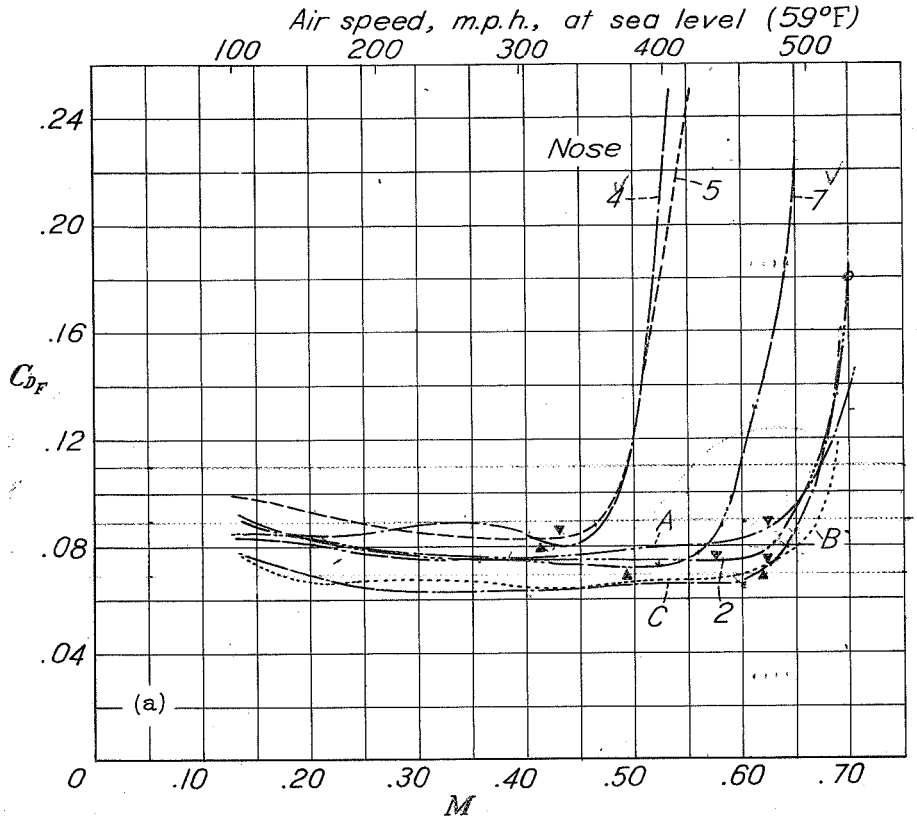

Figure 7,a

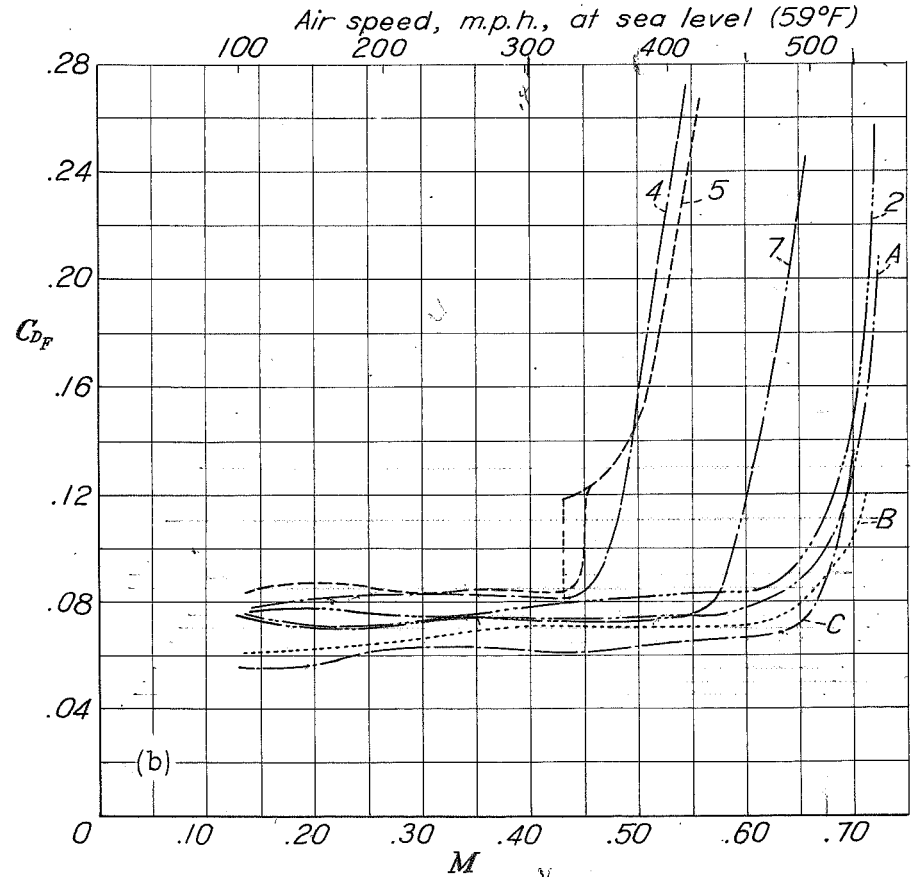

Figure 7,b

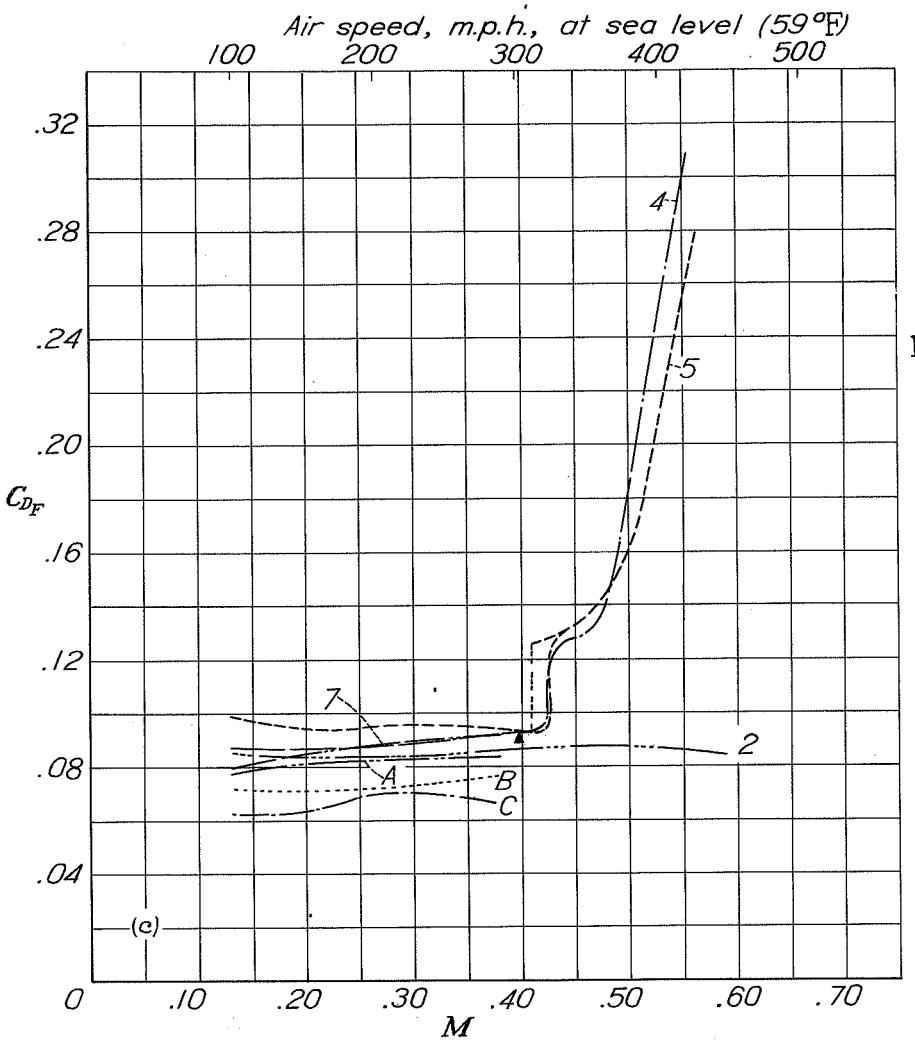

Figure 7,c

$\alpha = 1°$

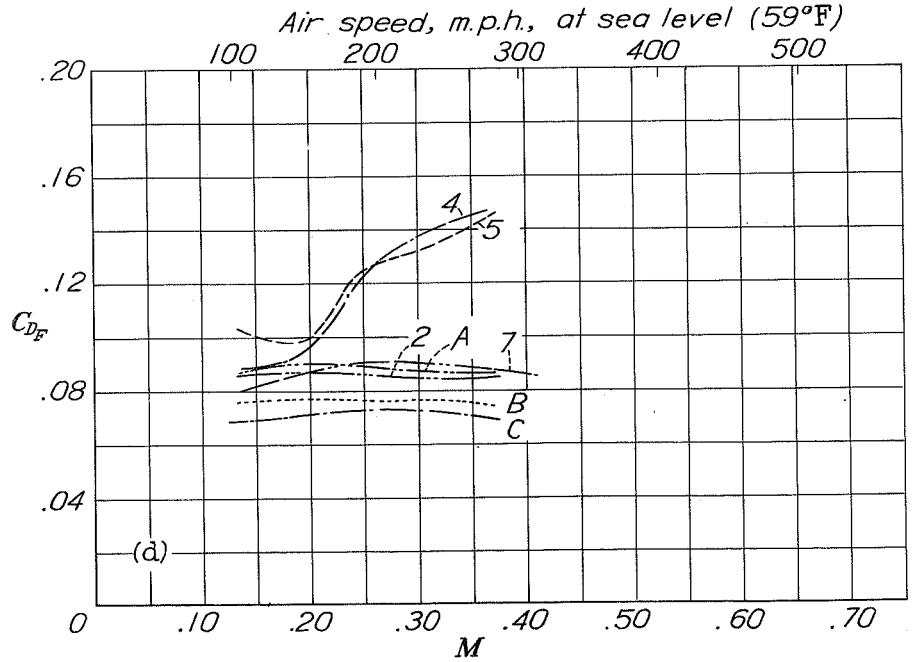

Figure 7,d

$\alpha = 2°$

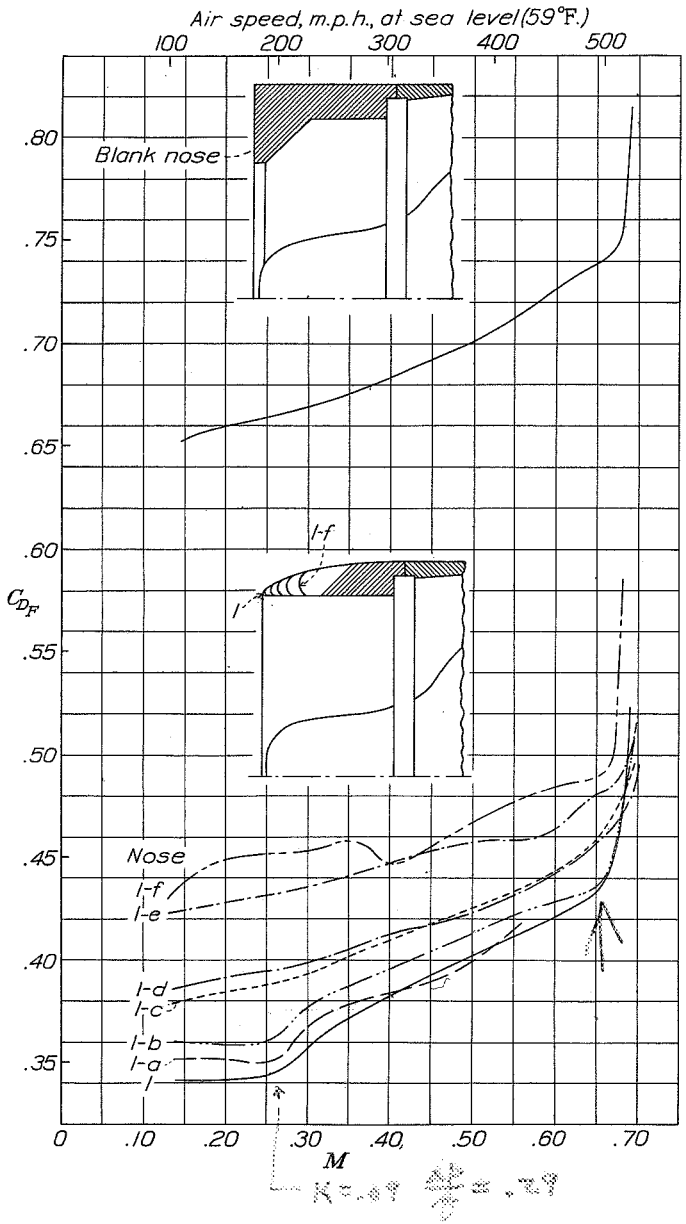

Figure 8

$\alpha = 0°$

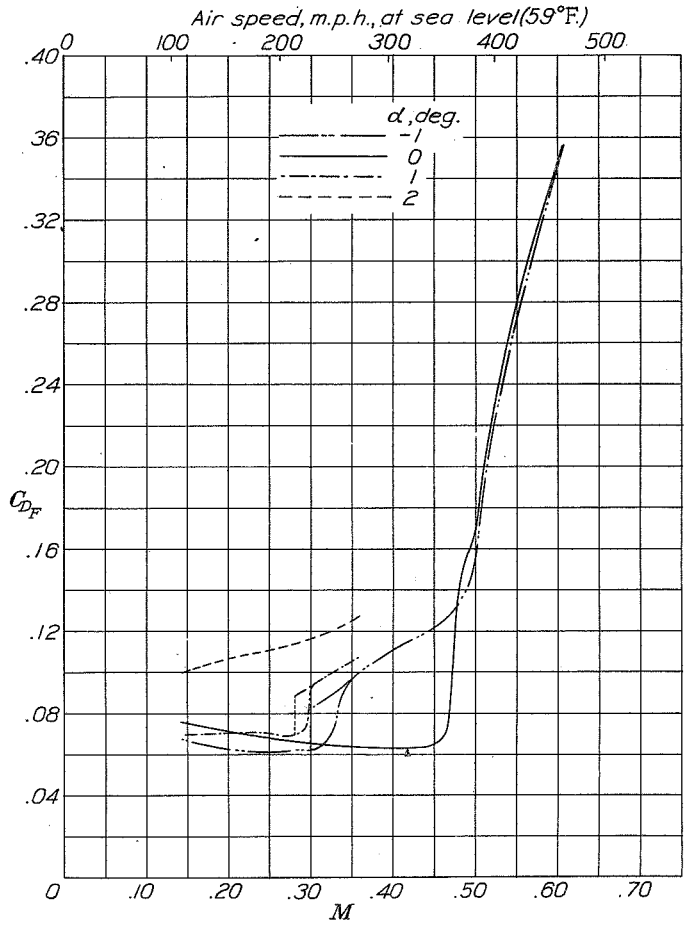

Figure 9

N.A.C.A.

Figs. 8,9

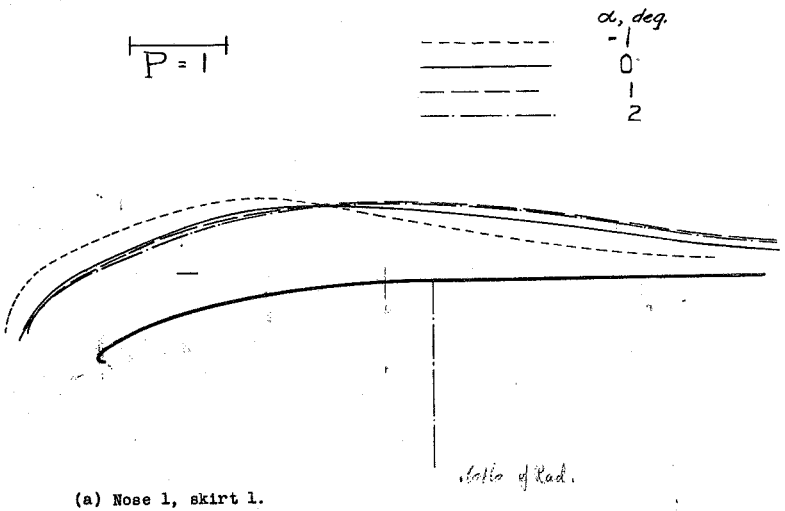

(a) Nose 1, skirt 1.

Figure 10. - Pressure distribution over top of cowlings. M_{∞} 0.30, except as noted.

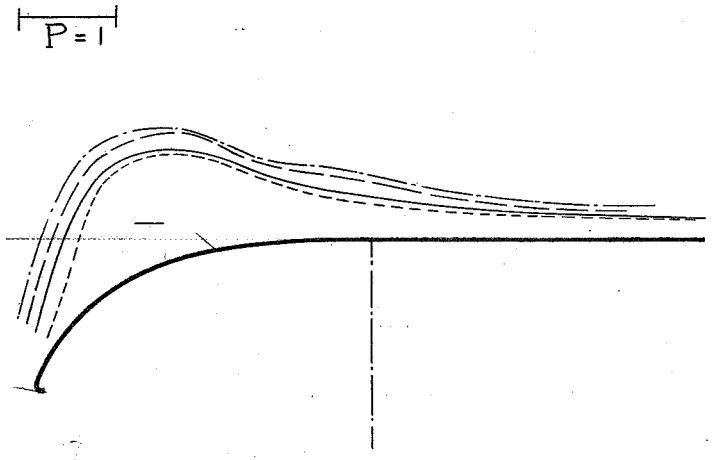

(b) Nose 2, skirt 1.

Figure 10. - Continued.

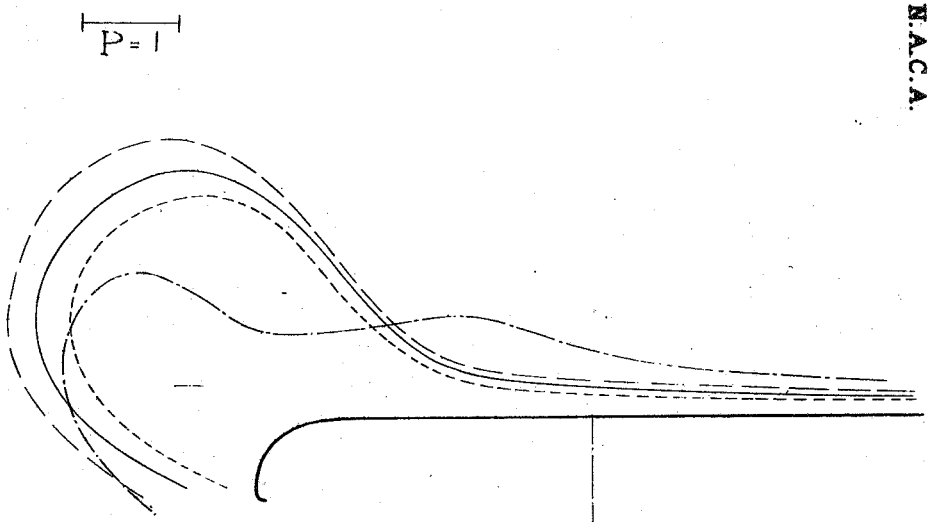

(c) Nose 4, skirt 1.

Figure 10. - Continued.

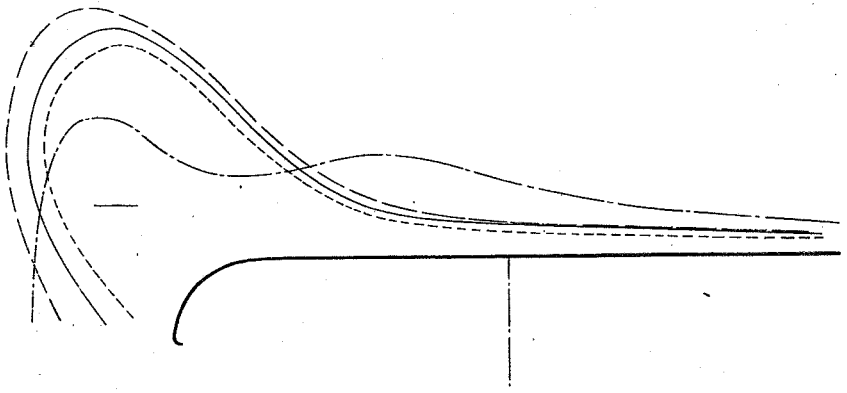

(d) Nose 5, skirt 1.

Figure 10. - Continued.

N.A.C.A.

Fig. 10.a,b,c,d

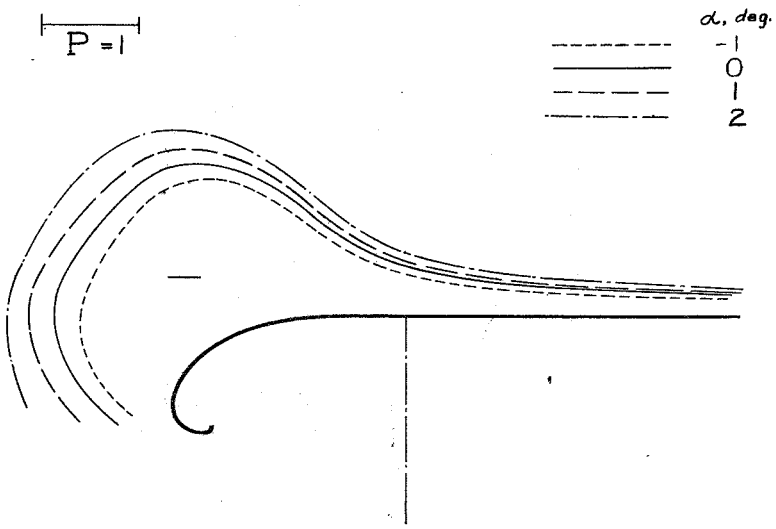

(e) Nose 7, skirt 1.

Figure 10. - Continued.

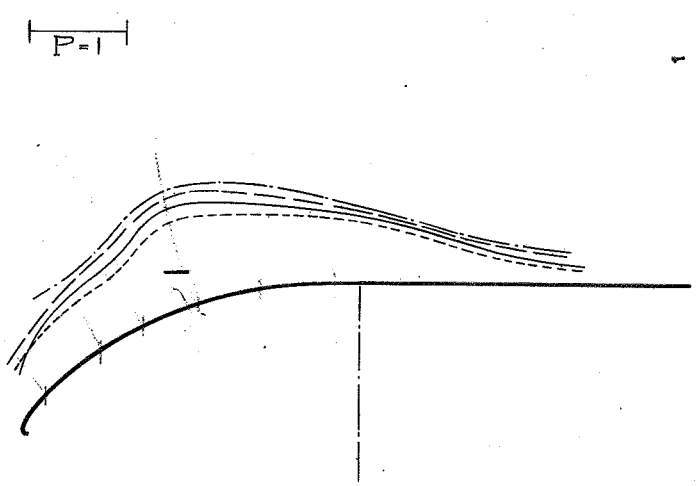

(f) Nose A, skirt 1.

Figure 10. - Continued.

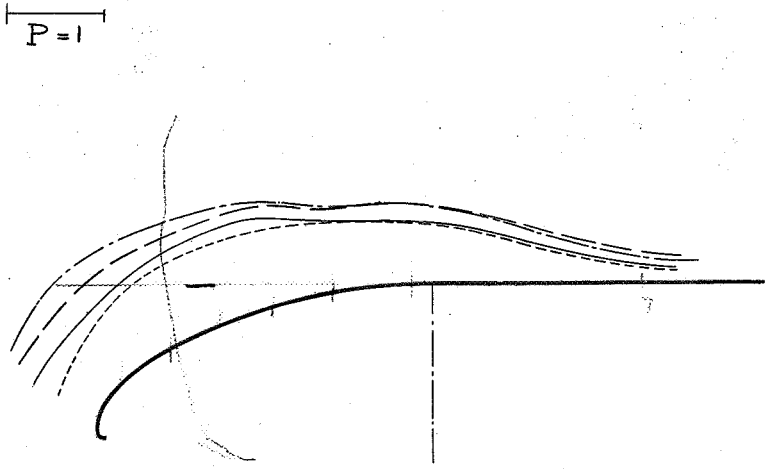

(g) Nose B, skirt 1.

Figure 10. - Continued.

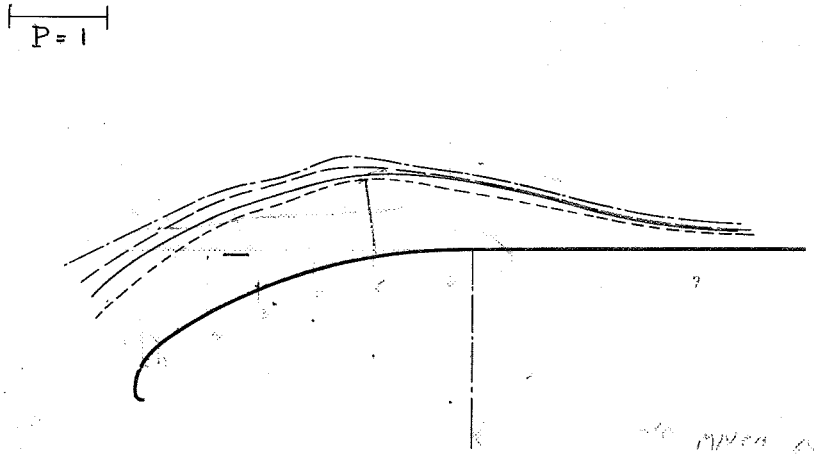

(h) Nose C, skirt 1.

Figure 10. - Continued.

Fig. 10.e,f,g,h

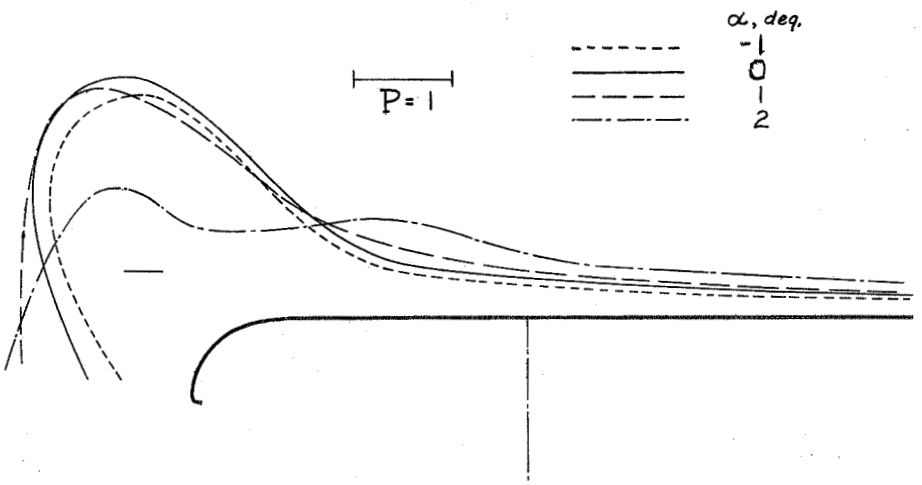

(i) Nose 5, skirt 2.

Figure 10. - Continued.

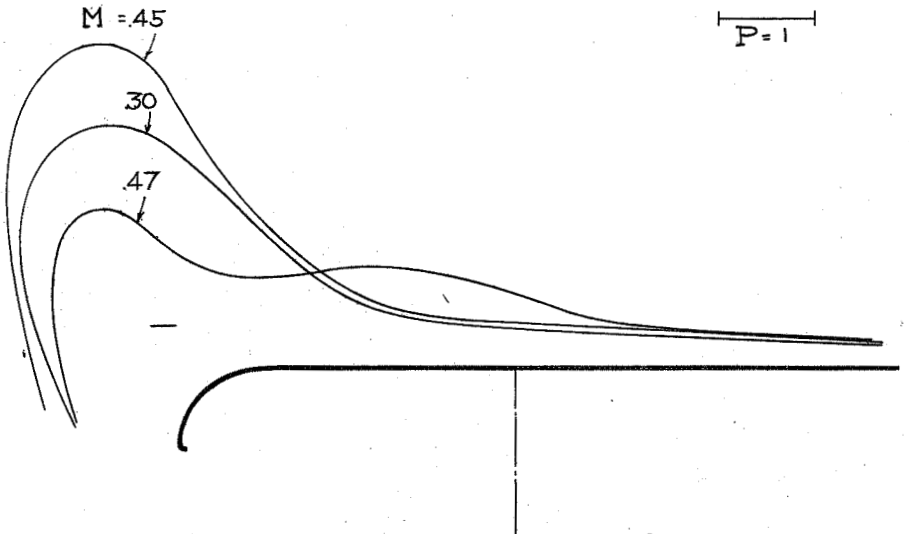

(j) Nose 5, skirt 2; critical M = 0.46; $\alpha = 0^{\circ}$.

Figure 10. - Continued.

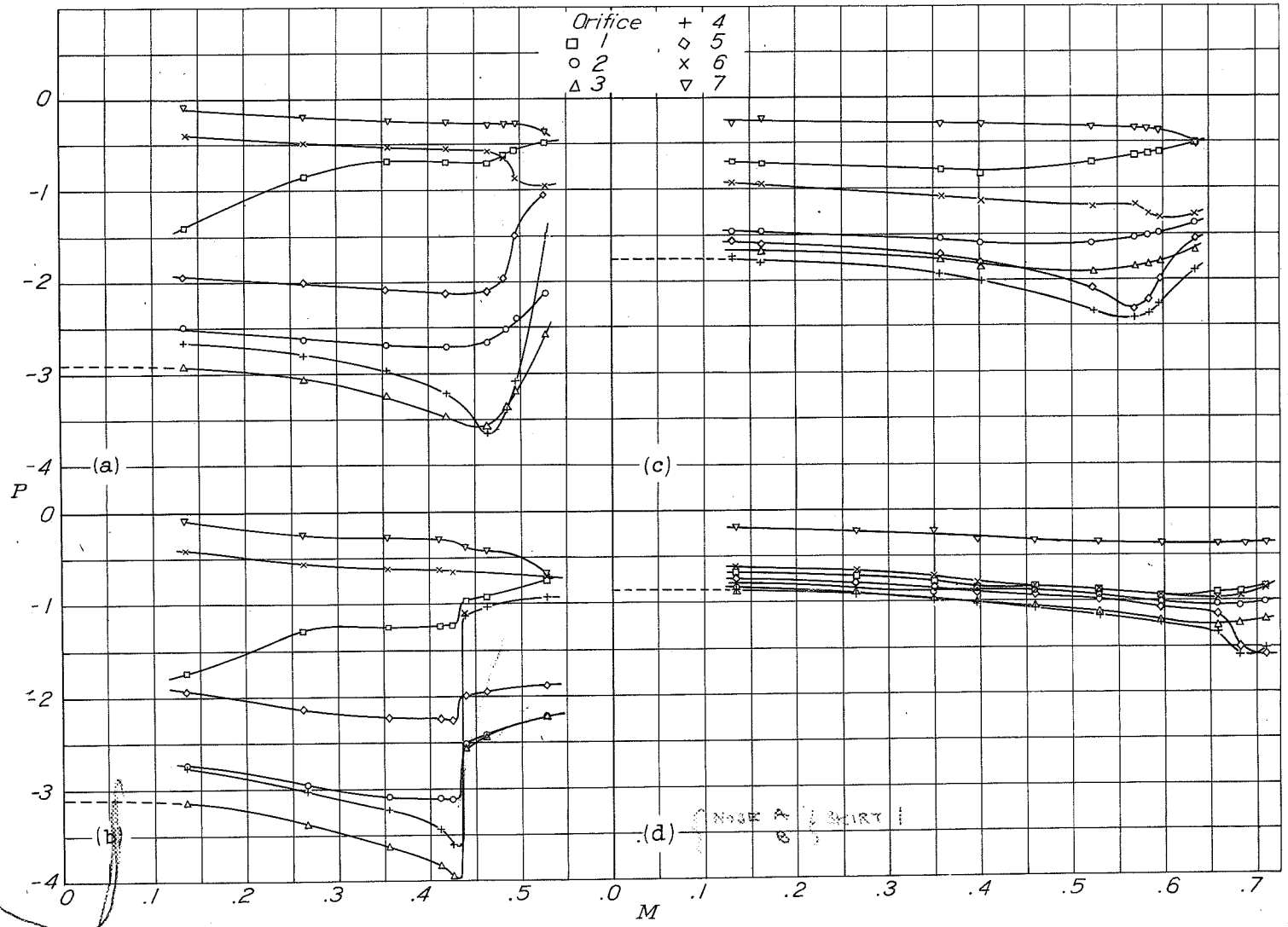

Figure 11

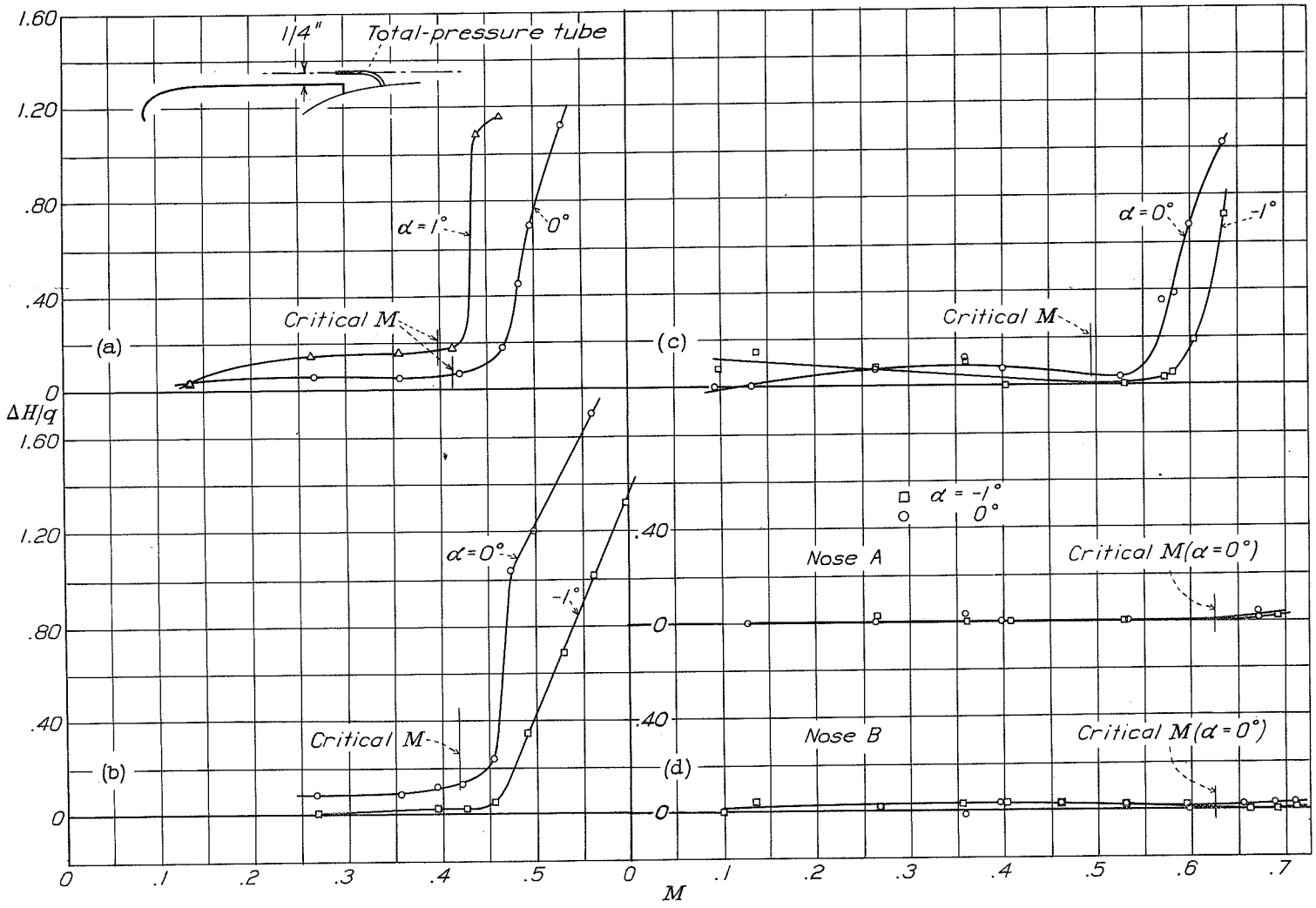
1/4"
Total-pressure tube
(a)
α = 1°
0°
Critical M
(b)
α = 0°
-1°
Critical M
(c)
α = 0°
-1°
Critical M
α = -1°
0°
Nose A
Critical M(α = 0°)
(d)
Nose B
Critical M(α = 0°)
ΔH/q
M
1.60
1.20
.80
.40
0
.1
.2
.3
.4
.5
.6
.7

Figure 12

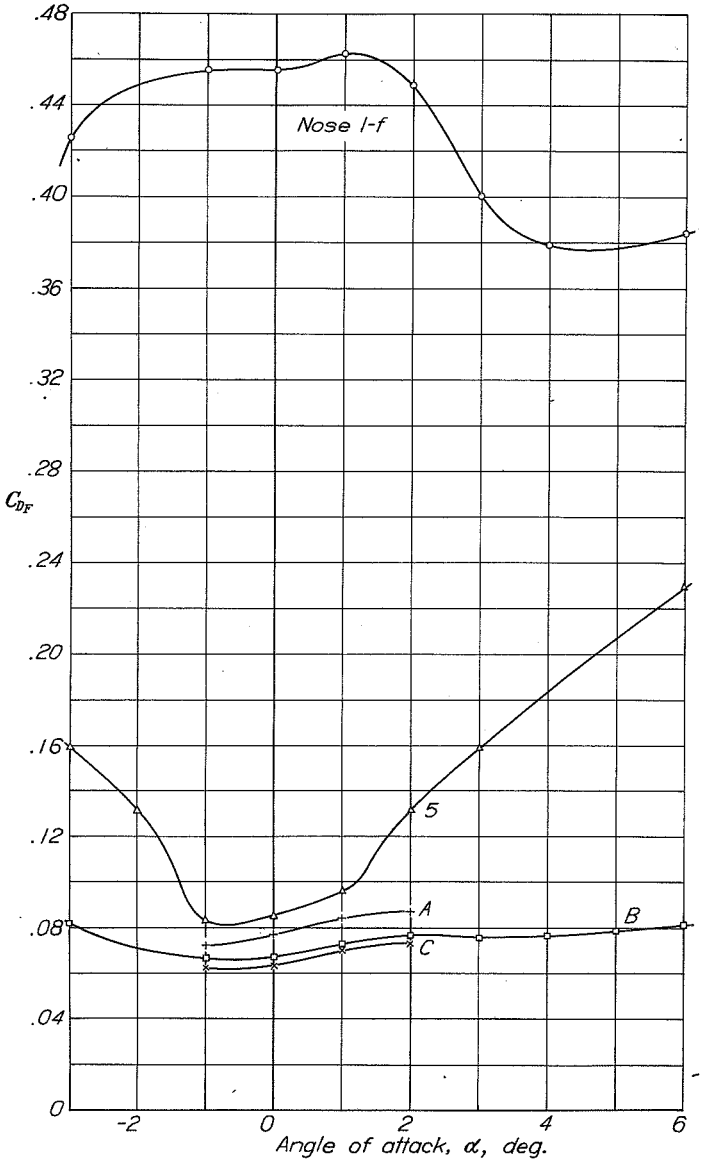

Figure 13

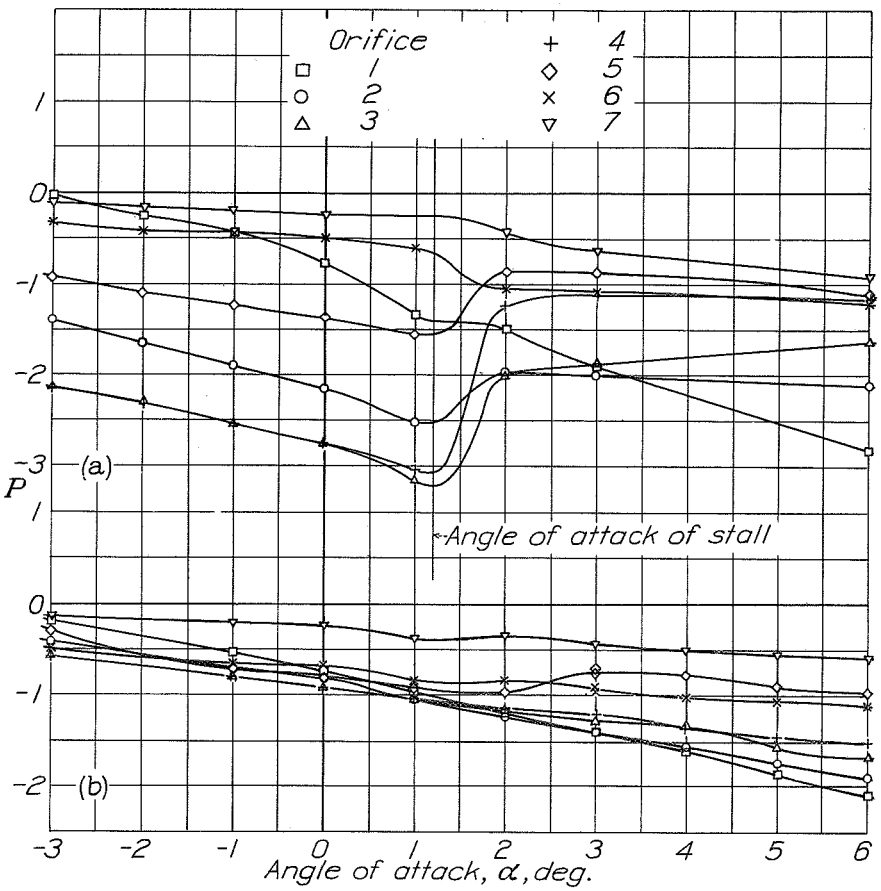

Figure 14

N.A.C.A.

Figs. 13, 14

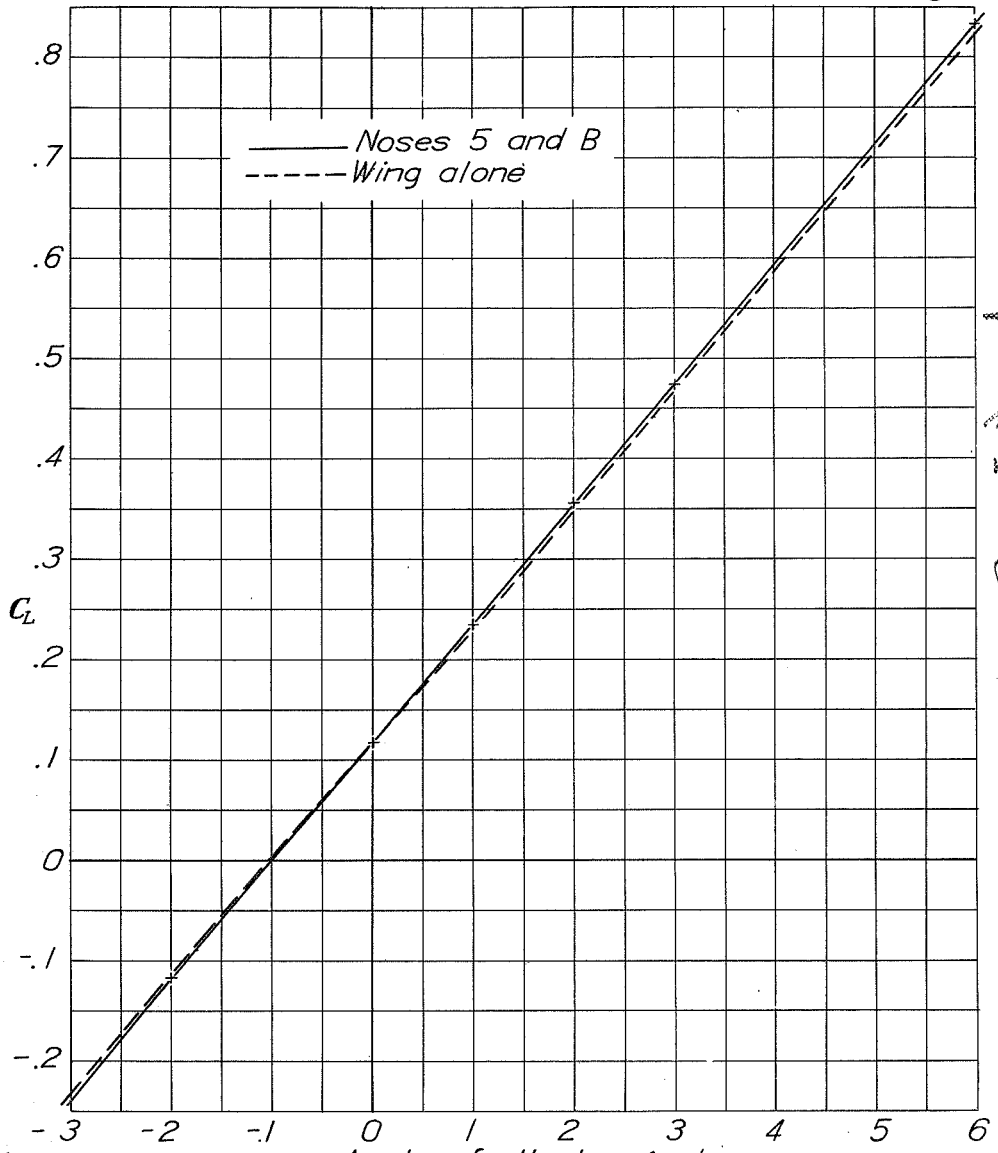

Effect of nacelle on wing C_L - uncorrected for tunnel-wall effect M = 0.30

Figure 15

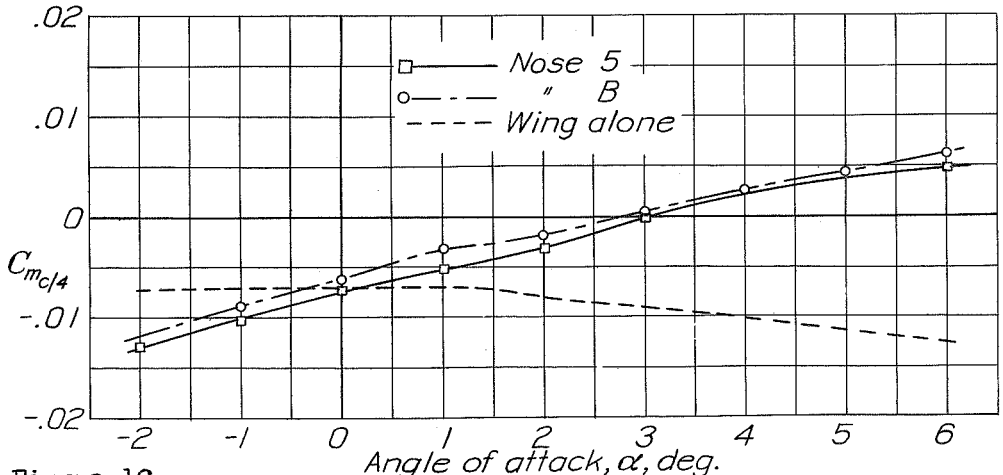

Figure 16

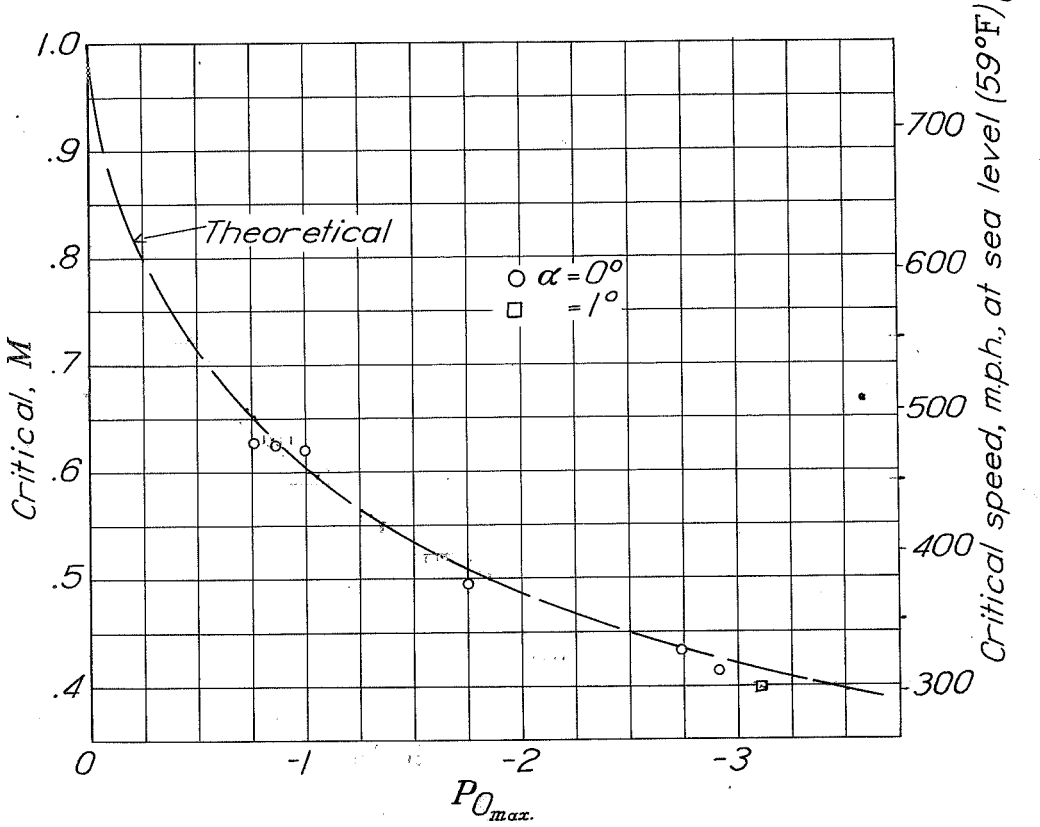

Figure 17

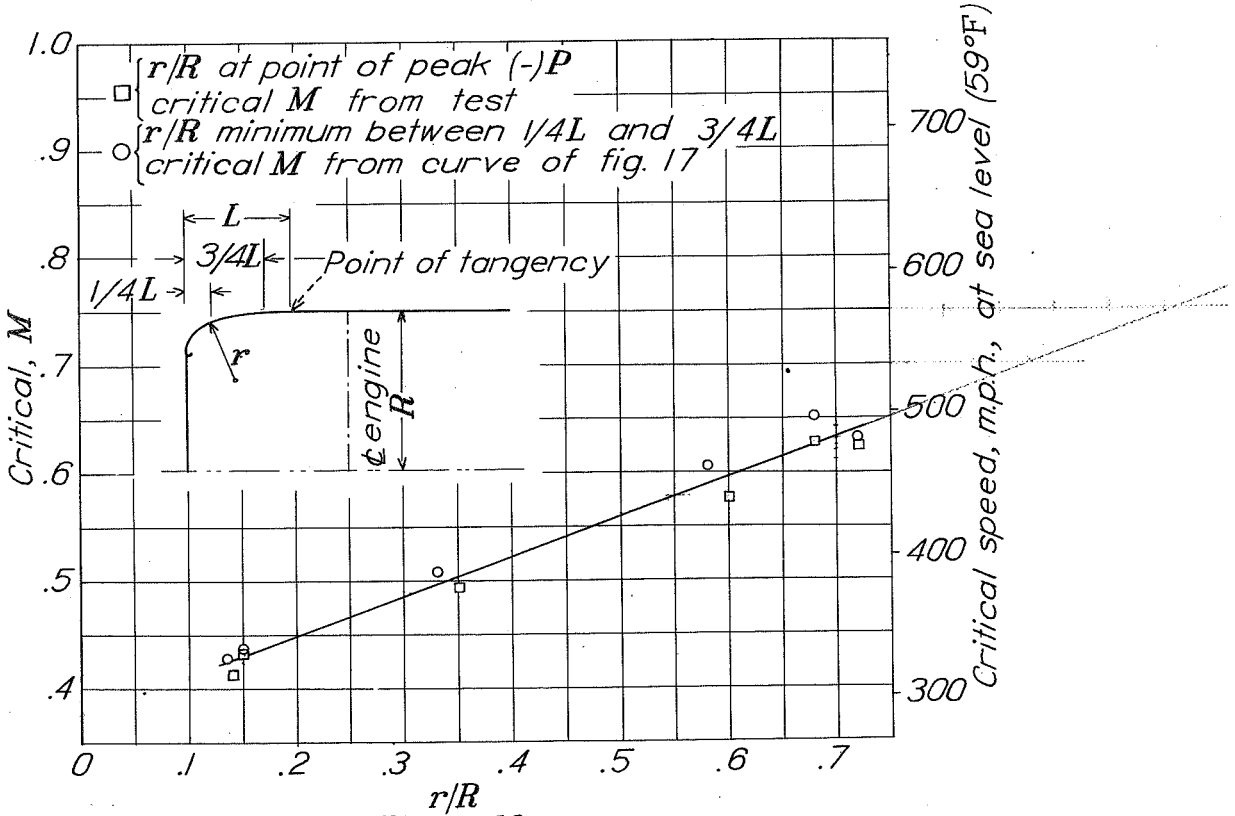

Figure 18

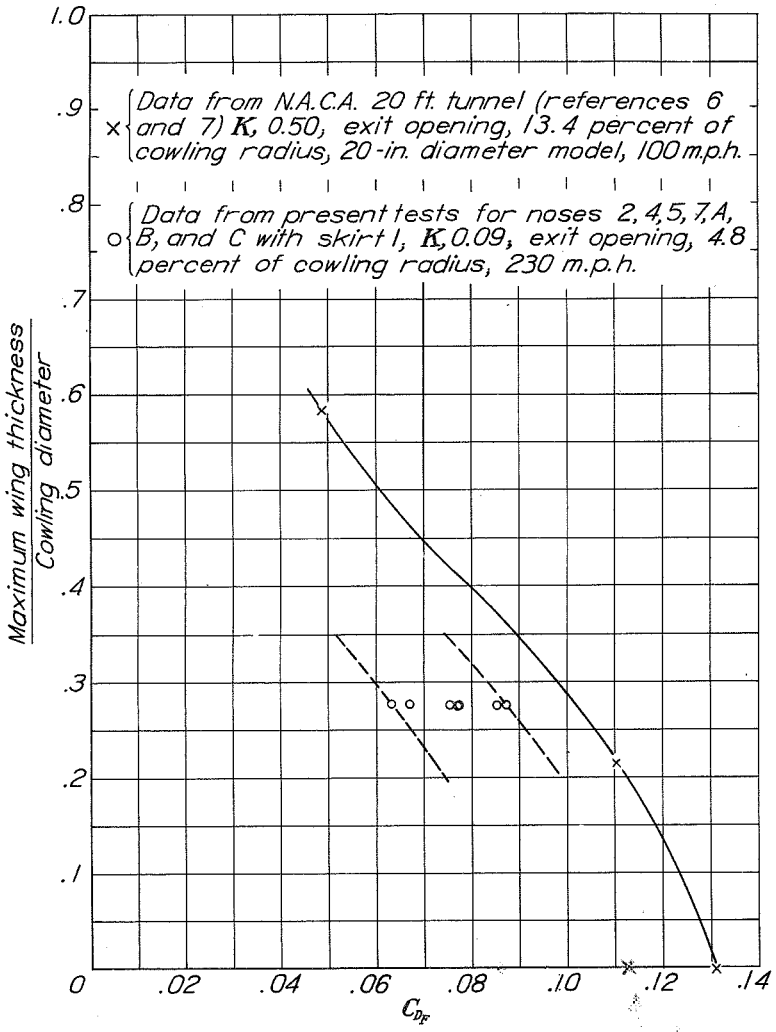

Figure 19

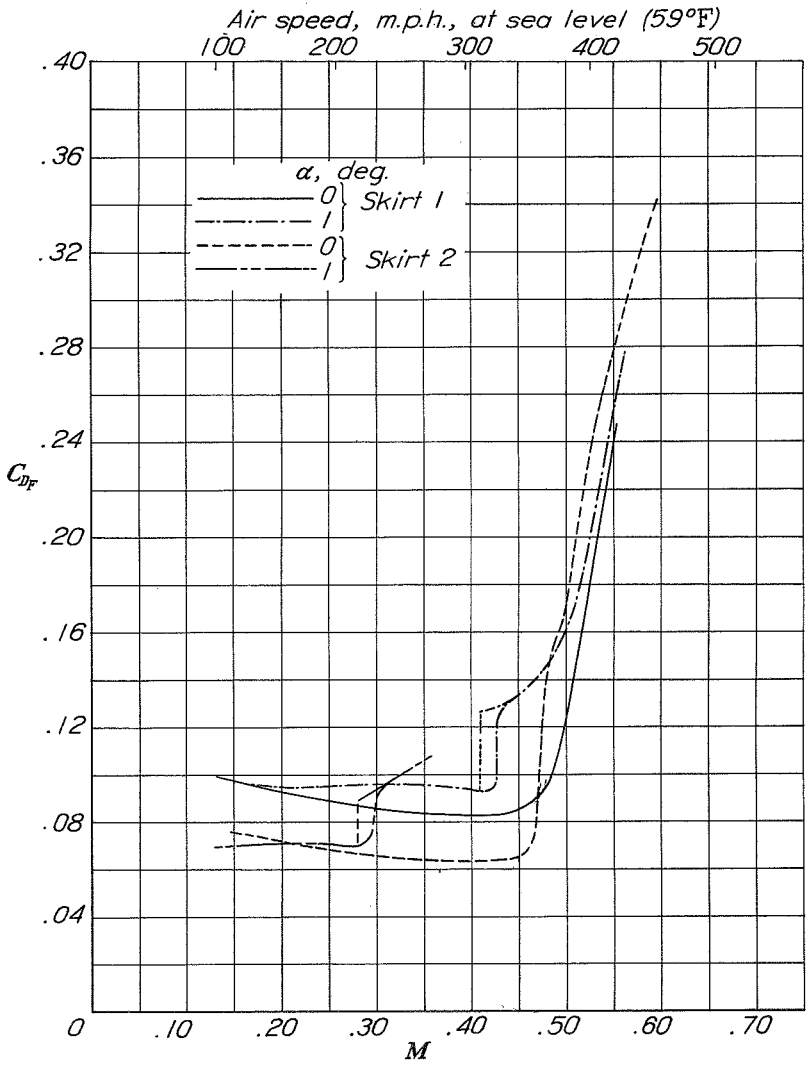

Figure 20

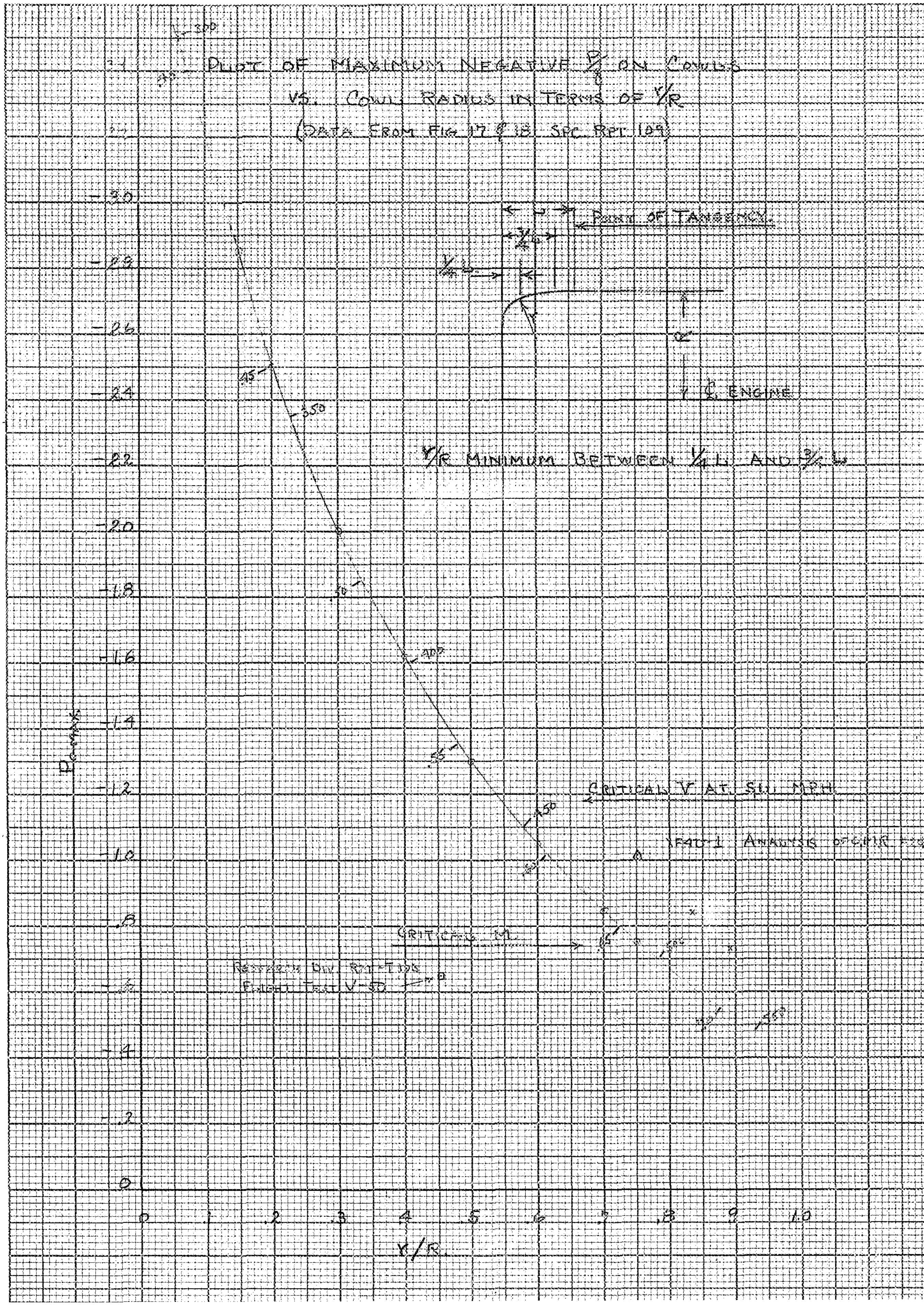

PLOT OF MAXIMUM NEGATIVE P/q ON COWLS
VS. COWL RADIUS IN TERMS OF Y/R
(DATA FROM FIG 17 & 18 SPC RPT 109)
POINT OF TANGENCY
℄ ENGINE
Y/R MINIMUM BETWEEN 1/4 L AND 3/4 L
CRITICAL V AT S.L. MPH
CRITICAL M
RESEARCH DIV. RPT-T105 FLIGHT TEST V-50
Y/R

Check of Research Rpt. T-103 Cond Max $-P/q$ against that obtained from Spc. Rpt. 109.

Drawing of pg. 34 min $r = 1.5$ in (ORB & WCS agree on 1.5)

$R = 23(.125) = 2.88$ $\qquad \frac{1.5}{12} = .125$

$r/R = \frac{1}{2.88} = .451$

P/q max $= -.650$ ✓ pg. 34 cond 0°

XF4U-1. Data from C.M.R. #24

Max. neg. $P/q = 1.01$ ($\alpha = -3.1°$ $C_L = 0$)

assume $r/R = .750$ obs. Cle. 4/18/39. Cond Fab for XF4U-1